

Article

Post-Synthesis Strategies to Prepare Mesostructured and Hierarchical Silicates for Liquid Phase Catalytic Epoxidation

Diana M. Gomes ¹, Patrícia Neves ^{1,*}, Margarida M. Antunes ¹, António J. S. Fernandes ²,
Martyn Pillinger ¹ and Anabela A. Valente ^{1,*}

¹ CICECO—Aveiro Institute of Materials, Department of Chemistry, University of Aveiro, 3810–193 Aveiro, Portugal

² i3N, Department of Physics, University of Aveiro, 3810–193 Aveiro, Portugal

* Correspondence: pneves@ua.pt (P.N.); atav@ua.pt (A.A.V.)

Abstract: Olefin epoxidation is an important transformation for the chemical valorization of olefins, which may derive from renewable sources or domestic/industrial waste. Different post-synthesis strategies were employed to introduce molybdenum species into mesostructured and hierarchical micro-mesoporous catalysts of the type TUD-1 and BEA, respectively, to confer epoxidation activity for the conversion of relatively bulky olefins (e.g., biobased methyl oleate, *DL*-limonene) to epoxide products, using *tert*-butyl hydroperoxide as an oxidant. The influences of (i) the type of metal precursor, (ii) type of post-synthesis impregnation method, (iii) type of support and (iv) top-down versus bottom-up synthesis methodologies were studied to achieve superior catalytic performances. Higher epoxidation activity was achieved for a material prepared via (post-synthesis) incipient wetness impregnation of MoO₂(acac)₂ (acac = acetylacetonate) on (pre-treated) siliceous TUD-1 and calcination; for example, methyl oleate was converted to the corresponding epoxide with 100% selectivity at 89% conversion (70 °C). Catalytic and solid-state characterization studies were conducted to shed light on material stability phenomena.

Keywords: catalytic epoxidation; olefins; porous materials; hierarchical zeolite; ordered mesoporous silica; molybdenum



Citation: Gomes, D.M.; Neves, P.; Antunes, M.M.; Fernandes, A.J.S.; Pillinger, M.; Valente, A.A. Post-Synthesis Strategies to Prepare Mesostructured and Hierarchical Silicates for Liquid Phase Catalytic Epoxidation. *Catalysts* **2022**, *12*, 1513. <https://doi.org/10.3390/catal12121513>

Academic Editors: Sébastien Leveneur, Vincenzo Russo and Pasi Tolvanen

Received: 2 November 2022

Accepted: 21 November 2022

Published: 25 November 2022

Publisher's Note: MDPI stays neutral with regard to jurisdictional claims in published maps and institutional affiliations.



Copyright: © 2022 by the authors. Licensee MDPI, Basel, Switzerland. This article is an open access article distributed under the terms and conditions of the Creative Commons Attribution (CC BY) license (<https://creativecommons.org/licenses/by/4.0/>).

1. Introduction

The epoxidation of olefins to epoxides is an important chemical transformation carried out in the industrial manufacturing of worldwide consumer goods such as, plastics, detergents, solvents, clothing, antifreeze, perfumes, drugs, etc. Olefins may derive from renewable sources of organic carbon [1] or domestic/industrial waste (e.g., used cooking oils, citrus residues, biorefinery byproducts), and thus their valorization via epoxidation processes may contribute to a sustainable biobased/circular economy.

The use of adequate catalysts, preferably heterogeneous ones, in olefin epoxidation processes is important to achieve high productivity. The requirements to be put on solid catalysts depend on several factors including the characteristics of the reactants. The most common olefins used for producing consumer products are the (fossil fuel-derived) commodity chemicals ethene and propene, which are very small molecules. However, olefins derived from biomass components include a larger set of relatively bulky molecules, such as unsaturated terpenes and fatty acids derived from vegetable oils. Hence, catalysts possessing high specific surface area and mesoporosity may facilitate the accessibility of the reactants to the active sites, enhancing the overall productivity. Regarding the type of oxidant, hydroperoxides such as hydrogen peroxide (H₂O₂) and *tert*-butyl hydroperoxide (TBHP) are preferred because they are readily available and relatively ecofriendly, as their coproducts are water and *tert*-butanol (which may be repurposed), respectively. These types of oxidants are used industrially, e.g., for the catalytic epoxidation of propene [2].

Whereas TBHP is commercialized in the form of concentrated aqueous or organic solutions, H_2O_2 is commercialized as less concentrated aqueous solutions because of its considerable instability and poorer solubility in organic media [3–6]. Hence, the use of TBHP may allow to reach high oxidant consumption efficiency (i.e., minimal unproductive decomposition of the oxidant). Moreover, avoiding excess water (added together with the oxidant) in the reaction media may prevent (i) competitive interactions between the reactants (olefin, oxidant) and water at the active sites, (ii) formation of biphasic liquid–liquid mixtures (which may suffer mass transfer limitations), and (iii) side reactions such as epoxide ring-opening via hydrolysis. Furthermore, H_2O_2 may also affect the catalyst stability, as opposed to TBHP [7,8].

Molybdenum-based catalysts are known to be effective for liquid phase olefin epoxidation with hydroperoxide oxygen donors. Hence, several types of molybdenum solid catalysts have been developed, such as carbon-based materials (e.g., graphene oxide), organic polymers, hybrids (e.g., metal–organic frameworks), metal oxides or mixed metal oxides (e.g., silica, zirconia, titania, alumina, clays), etc. [9,10]. Fully inorganic catalysts seem attractive in that they may possess relatively high thermal and chemical stabilities compared with carbon-containing catalysts (e.g., the latter may chemically degrade in oxidizing media, thermally decompose during calcination to regenerate the thoroughly used catalyst, etc.). Yet, important challenges such as catalyst deactivation phenomena (e.g., metal leaching) and/or poorer catalytic activity of the solid catalysts compared with their homogeneous counterparts, continue to drive scientific research in this field to develop more efficient heterogeneous epoxidation catalysts [7,11–18].

Regarding fully inorganic porous materials, ordered mesoporous silicas and zeolites (crystalline aluminosilicates used in oil refining and petrochemical processes for decades) are relatively robust, versatile and possess high specific surface area. Specifically, ordered mesoporous silica/silicates of the type TUD-1 are attractive in that they are hydrothermally synthesized via (green) non-surfactant routes (as opposed to e.g., MCM-41), and do not require relatively expensive polymeric organic templates (e.g., Pluronic P123 triblock copolymer used for synthesizing SBA-15) [19,20]. According to the literature, Mo-containing TUD-1 (Si/Mo = 100) prepared via hydrothermal synthesis using the polynuclear molybdenum precursor $(NH_4)_6Mo_7O_{24}$ catalyzed the epoxidation of cyclohexene with TBHP, although with limited stability [13]. More recently, molybdena doped titania was supported on TUD-1 silica and aluminosilicate supports, and tested for olefin epoxidation with H_2O_2 ; catalyst stability was not addressed [21,22].

Zeolites are microporous materials, but they may be modified to introduce mesoporosity, resulting in hierarchical micro-mesoporous zeotypes. Literature studies suggested that the large pore BEA topology may be more effective for olefin epoxidation with TBHP than the medium pore MFI topology, partly due to the more limited micropore sizes of the latter [23–25]. On the other hand, a literature study indicated that molybdenum impregnated on siliceous BEA (using $MoCl_5$ in dichloromethane) was unstable in the presence of H_2O_2 (not explored as catalyst) [7]. Niederer and Hölderich [17] prepared Mo-containing BEA via gas phase isomorphous substitution for olefin epoxidation with TBHP; this catalyst synthesis strategy involved the pre-synthesis of boron-containing BEA, followed by the introduction of $MoOCl_3$ at a high temperature of 240 °C. To the best of our knowledge, no olefin epoxidation studies are reported in the literature for Mo-containing intracrystalline hierarchical BEA zeotypes.

In this work, fully inorganic molybdenum-containing catalysts possessing mesoporosity were investigated for the liquid phase epoxidation of relatively bulky olefins, using TBHP as oxidant (Figure 1). Specifically, the catalytic supports were (pre-treated) TUD-1 and a hierarchical micro/mesoporous BEA zeotype (hierBEA). These materials were furnished with molybdenum sites via post-synthesis strategies, which may allow better control over the metal loading in relation to, for example, the sol-gel method (not all metal in the synthesis gel may be incorporated into the final material). Post-synthesis strategies which avoid the use of solvents or that require minimal amounts of solvent, are economically and

environmentally attractive, which is the case of incipient wetness impregnation (IWI) and solid-state impregnation (SSI) used in the present study. The type of molybdenum precursor is another important factor. In this respect, non-halide precursors may be preferable to halide-containing ones to avoid the formation of halogenated byproducts and toxic waste, and contaminations of the catalyst. On the other hand, mononuclear molybdenum precursors may be preferable to polynuclear ones for achieving uniform metal distributions [15]. Hence, the following non-halide precursors were chosen: mononuclear $\text{MoO}_2(\text{acac})_2$ and $(\text{NH}_4)_2\text{MoO}_4$, and, for comparison, the polynuclear precursor $(\text{NH}_4)_6\text{Mo}_7\text{O}_{24}$. The prepared materials promoted the epoxidation of relatively bulky C8 olefins (*cis*-cyclooctene, 1-octene, *trans*-2-octene) and biobased olefins (methyl oleate, *DL*-limonene), leading to relatively high epoxide yields at 70 °C. The post-synthesis strategy led to higher activity than the sol-gel method (TUD-1 family), and, on the other hand, the type of post-synthesis impregnation method (SSI versus IWI), type of support (TUD-1 versus BEA) and molybdenum precursor influenced the catalytic activity. Higher epoxidation activity was reached for Mo-TUD(IWI-acac) prepared via IWI of $\text{MoO}_2(\text{acac})_2$ on pre-treated TUD-1 and calcination; for example, methyl oleate was converted to the corresponding epoxide in 100% selectivity at 89% conversion (70 °C). Catalytic and solid-state characterization studies shed light on the material stability aspects.

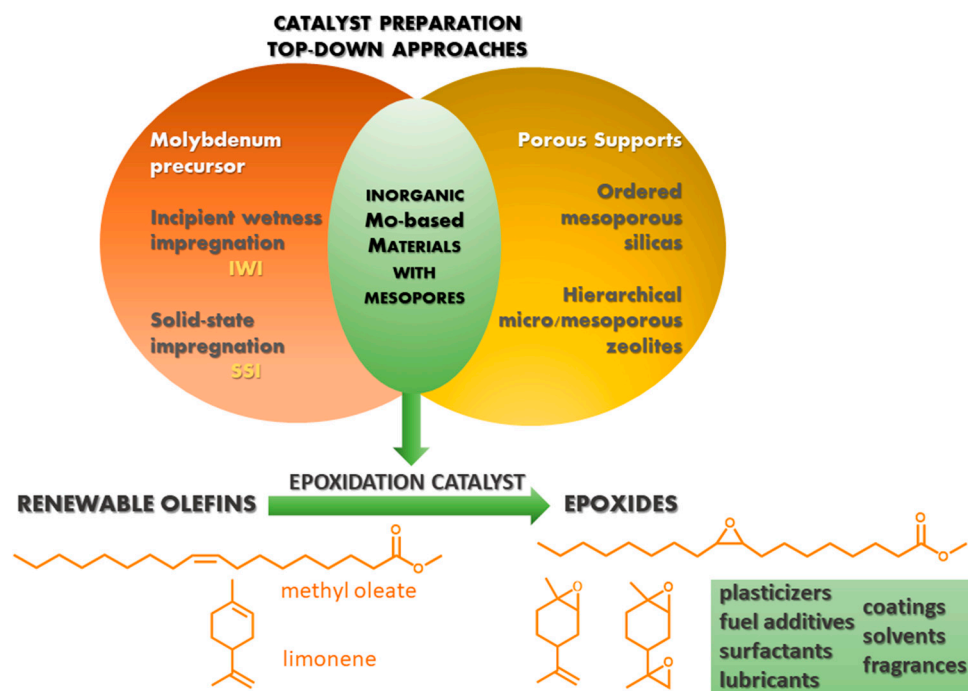


Figure 1. Chemical valorization of olefins to epoxides using fully inorganic silicate catalysts possessing mesoporosity, prepared via top-down strategies.

2. Results and Discussion

2.1. Characterization of the Materials

2.1.1. Ordered Mesoporous TUD-1 Type Materials

The Mo-containing TUD-1(IWI) type materials were prepared via pretreatment of (pre-made) siliceous TUD-1 (giving TUD-1(PT)), followed by incipient wetness impregnation (IWI) and calcination, using the metal precursors $\text{MoO}_2(\text{acac})_2$ (denoted acac), $(\text{NH}_4)_2\text{MoO}_4$ (denoted amm) and $(\text{NH}_4)_6\text{Mo}_7\text{O}_{24}$ (denoted ahm), which gave Mo-TUD(IWI-acac), Mo-TUD(IWI-amm) and Mo-TUD(IWI-ahm), respectively. For comparison with the IWI method, Mo-TUD(SSl-acac) was prepared via solid-state impregnation (SSI) of the precursor acac (keeping the Mo loading constant).

The pretreated TUD-1 possessed an enhanced concentration of silanol groups (increased from $0.79 \text{ mmol}_{\text{SiOH}} \text{ g}^{-1}$ for TUD-1 to $1.85 \text{ mmol}_{\text{SiOH}} \text{ g}^{-1}$ for TUD-1(PT), based on

TGA), which may advantageously enhance the surface reactivity in the IWI process. Notably, for a 2 wt% Mo loading ($0.21 \text{ mmol}_{\text{Mo}} \text{ g}^{-1}$), $1.85 \text{ mmol}_{\text{SiOH}} \text{ g}_{\text{TUD-1(PT)}}^{-1}$ corresponds to an available molar ratio SiOH/Mo of ca. 9. With the impregnation of molybdenum, SiOH/Mo decreased to less than unity. Since the IWI and SSI methodologies do not require downstream filtration and/or material washing processes, the amount of molybdenum added to the support ($0.21 \text{ mmol}_{\text{Mo}} \text{ g}^{-1}$, Si/Mo \cong 70) may be totally retained in the final materials.

For comparison with the post-synthesis strategies, Mo-TUD-1(HT) was hydrothermally synthesized (under static conditions) from a synthesis mixture possessing Si/Mo = 70. However, the final material possessed Si/Mo = 149 ($0.08 \text{ mmol}_{\text{Mo}} \text{ g}^{-1}$, based on ICP-OES), suggesting that a significant fraction of molybdenum was not incorporated in the final material.

The PXRD patterns of all TUD-1 type materials showed a very broad peak in the range $18\text{--}30^\circ 2\theta$ associated with amorphous silica, in agreement with the literature for TUD-1 type materials (Figure 2 and Figure S1a) [19]. A peak centered at ca. $3.5\text{--}4^\circ 2\theta$ may be attributed to the mesostructured, three-dimensional sponge-like pore system of these types of materials [19]. Molybdenum oxide (bulk MoO_3) exhibited sharp reflections (reference code: 04-015-7146) which were not verified for the molybdenum-containing TUD-1 type materials. Hence, the latter did not possess a crystalline MoO_3 phase.

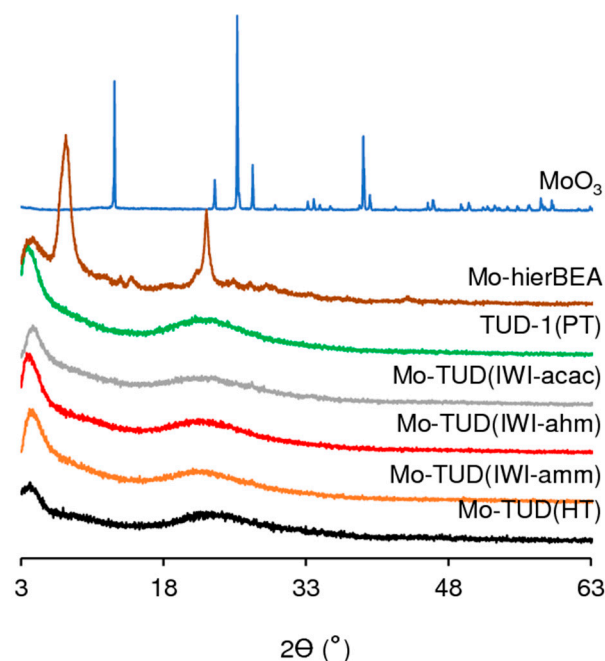


Figure 2. PXRD patterns of the prepared materials and, for comparison, bulk MoO_3 .

The SEM images showed micron-size particles of irregular morphology, and the elemental mappings showed uniform Mo and Si distributions (exemplified for Mo-TUD(IWI-acac) and Mo-TUD(HT) in Figure 3a,b).

All TUD-1 type materials exhibited type IV N_2 sorption isotherms, with a hysteresis loop (Figure 4a and Figure S1b) characteristic of mesoporous materials [26,27]. The specific surface areas were in the range $318\text{--}485 \text{ m}^2 \text{ g}^{-1}$ (Table 1) and the pore size distribution curves presented a maximum in the range $8.2\text{--}8.5 \text{ nm}$, excluding Mo-TUD(HT) which possessed larger mesopores (ca. 18.3 nm) (inset of Figure 4a and Figure S1b). The incorporation of molybdenum via IWI or SSI led to a reduction of S_{BET} , especially for Mo-TUD(IWI-ahm) which was prepared using the polynuclear precursor $(\text{NH}_4)_6\text{Mo}_7\text{O}_{24}$ (denoted ahm) and for Mo-TUD(SSI-acac) prepared via SSI.

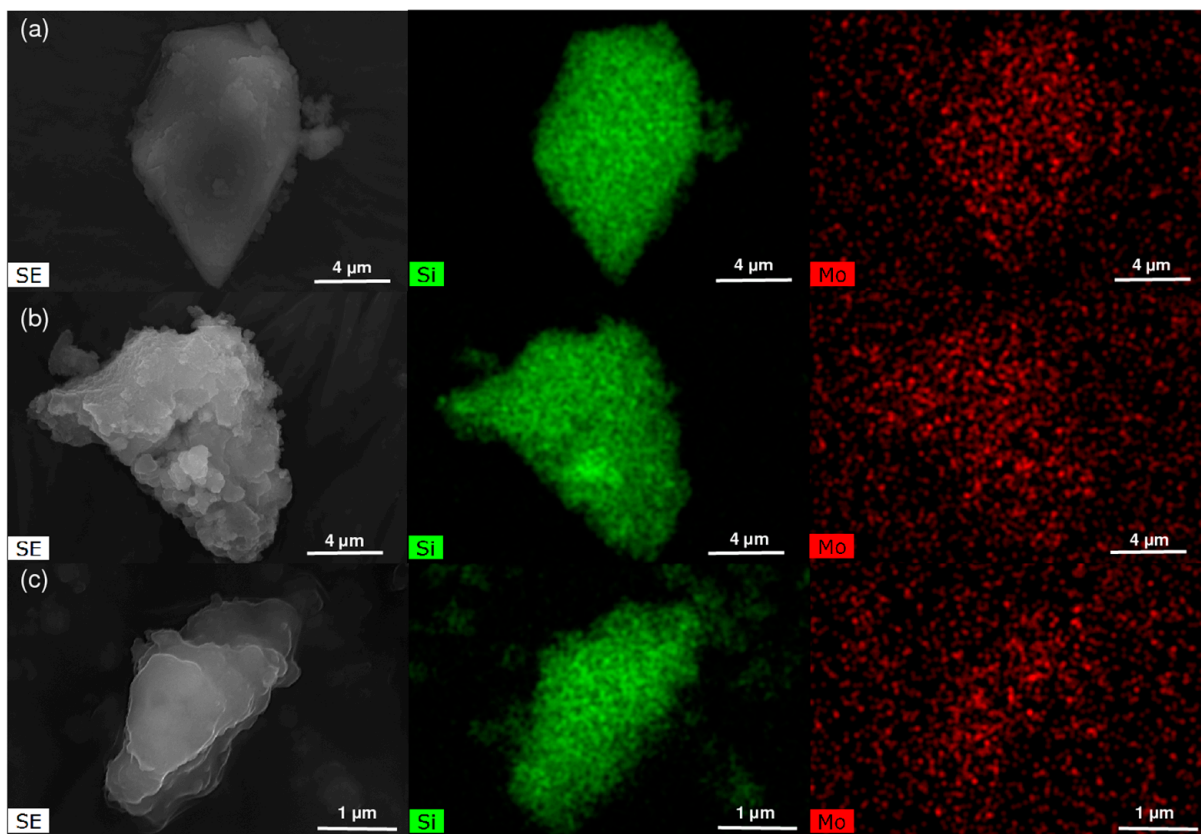


Figure 3. SEM images and elemental mappings (Si (green); Mo (red)) of Mo-TUD(IWI-acac) (a), Mo-TUD(HT) (b), and Mo-hierBEA (c).

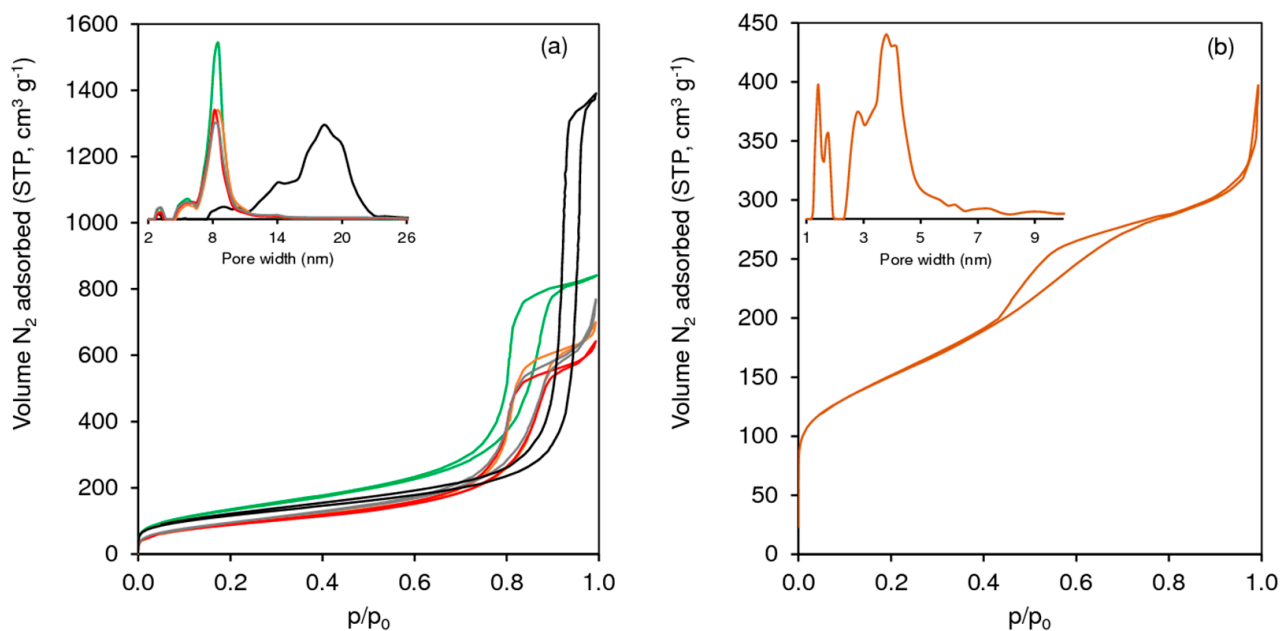


Figure 4. Nitrogen sorption isotherms at $-196\text{ }^{\circ}\text{C}$ of (a) TUD-1(PT) (green), Mo-TUD(IWI-acac) (grey), Mo-TUD(IWI-ahm) (red), Mo-TUD(IWI-amm) (orange), Mo-TUD(HT) (black), and (b) Mo-hierBEA. The insets show the respective pore size distributions (with matching colors).

Table 1. Composition and textural properties of the prepared materials.

Sample	Mo ¹ (mmol _{Mo} g ⁻¹)	S _{BET} ² (m ² g ⁻¹)	V _p ³ (cm ³ g ⁻¹)	D _p ⁴ (nm)
TUD-1	-	471	1.23	8.5
TUD-1(PT)	-	485	1.24	8.5
Mo-TUD(IWI-acac)	0.21	355	1.19	8.2
Mo-TUD(IWI-amm)	0.21	398	1.08	8.5
Mo-TUD(IWI-ahm)	0.21	322	0.99	8.2
Mo-TUD(SSI-acac)	0.21	318	0.74	8.2
Mo-TUD(HT)	0.08 ⁵	418	2.15	18.3
hierBEA ⁶	-	759 (468) ⁶	0.73 (0.12) ⁶	2.5–5 ⁶
Mo-hierBEA	0.21	532 (427)	0.61 (0.05)	2.5–5

¹ Mo loading of the material. ² For the TUD-1 family, S_{BET} coincides with the mesopore surface area; for the BEA family, the mesopore surface area is indicated in parenthesis. ³ For TUD-1 type materials, the total pore volume (V_p) equals the mesopore volume (i.e., the materials do not possess measurable micropore volume); for BEA type materials, V_p is the sum of micro- and mesopore volume (the micropore volume (V_{micro}) is indicated in parenthesis). ⁴ Mesopore size range (2–50 nm); the BEA materials also exhibited a micropore size distribution. ⁵ Based on ICP-OES (Si/Mo = 149). ⁶ Data reported in reference [28].

The materials with and without molybdenum exhibited similar ATR FT-IR spectra, which were different from that of bulk MoO₃ (Figure 5a). The silicates essentially exhibited bands associated with (i) surface silanol groups or Si-O polarized by the transition metal (Si-O bond stretching at ca. 970 cm⁻¹), and (ii) the siloxane framework (Si-O rocking vibration (ca. 440 cm⁻¹); symmetric (ca. 797 cm⁻¹) and asymmetric (ca. 1060 cm⁻¹) vibrations of Si-O-Si bonds) [29–32]. Other bands associated with Mo species were not clearly distinguished due to the predominating IR bands associated with the siliceous support.

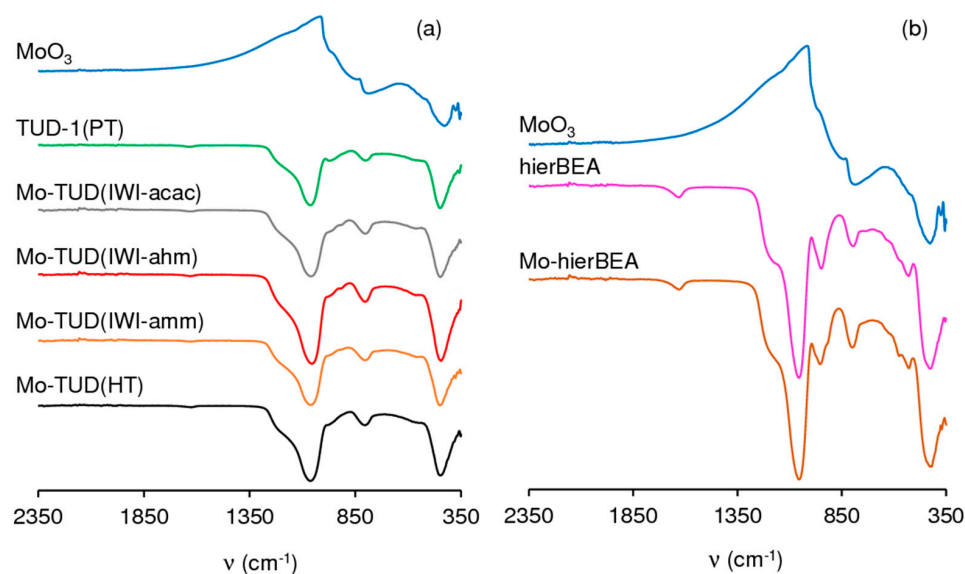


Figure 5. ATR FT-IR spectra of (a) TUD-1 type and (b) BEA type materials prepared. For comparison, the spectrum of bulk MoO₃ is included in (a,b).

The diffuse reflectance UV-Vis (DR UV-vis) spectrum of TUD-1(PT) was featureless, whereas the molybdenum-containing materials exhibited overlapping bands centered at ca. 215, 250 and 300 nm (Figure 6). The bands up to 250 nm may be due to isolated (mononuclear) molybdenum species, such as tetracoordinated monooxo- (Mo(=O)) and/or dioxomolybdenum (Mo(=O)₂) sites [33–36]. A shoulder at ca. 300 nm, may be due to the presence of some molybdenum species possessing Mo-O-Mo groups [33,35,36]. Bulk MoO₃ exhibited a main broad band centered at ca. 354 nm, in agreement with literature data [33–38], which was very different from the spectra of the TUD-1 type materials.

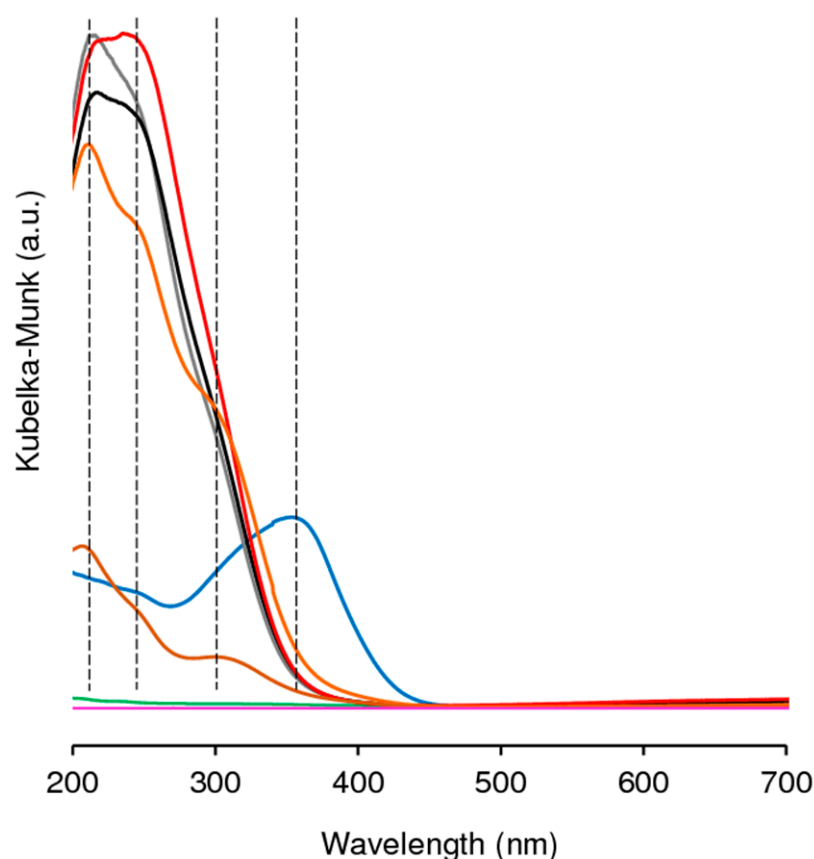


Figure 6. DR UV-vis spectra of TUD-1(PT) (green, close to baseline), Mo-TUD(IWI-acac) (black), Mo-TUD(IWI-ahm) (red), Mo-TUD(IWI-amm) (grey), Mo-TUD(HT) (orange), hierBEA (pink, close to baseline), Mo-hierBEA (brown), and for comparison, bulk MoO₃ (blue). Dashed lines signalize the bands at ca. 215, 250 and 300 nm, and 354 nm.

Figure 7 shows the Raman spectra of the TUD-1 type materials and, for comparison, the results for bulk MoO₃ are included. Bulk MoO₃ exhibits an intense band at ca. 820 cm⁻¹ (assignable to ν OMo₂), and weaker bands at ca. 663 cm⁻¹ (assignable to ν OMo₃ [39,40]) and 995 cm⁻¹ (stretching mode of terminal Mo=O groups [39]), in agreement with literature data [7,41]. The Raman spectrum of TUD-1(PT) was featureless, which may be partly due to strong fluorescence. The spectra of Mo-TUD(IWI-acac) and Mo-TUD(IWI-amm) were similar, as well as those of Mo-TUD(IWI-ahm) and Mo-TUD(HT), although the two sets of materials exhibited different spectral features. Mo-TUD(IWI-ahm) and Mo-TUD(HT) exhibited a band at ca. 820 cm⁻¹ and weak bands at ca. 660–670 cm⁻¹ and 982–989 cm⁻¹, which (by comparison with bulk MoO₃) are assignable to higher nuclearity molybdenum species [13,42]. Since PXRD did not show any peaks of crystalline molybdenum oxide phases, the supported higher nuclearity molybdenum species may be very small entities, e.g., dinuclear species or clusters. On the other hand, for Mo-TUD(IWI-amm) and Mo-TUD(IWI-acac), the Raman bands associated with bulk MoO₃ were not clearly distinguished, suggesting that these materials possess relatively low nuclearity Mo species. The overlapping bands in the range ca. 950–965 cm⁻¹ of the TUD-1 type materials, may include a band at ca. 958 cm⁻¹ assignable to the stretching mode of terminal Mo=O groups, with a possible contribution of Si-O stretching of defect sites containing molybdenum [16]. Overall, the materials may possess both mono- and polynuclear Mo species, but Mo-TUD(IWI-acac) and Mo-TUD(IWI-amm) seem to essentially possess relatively low nuclearity Mo species.

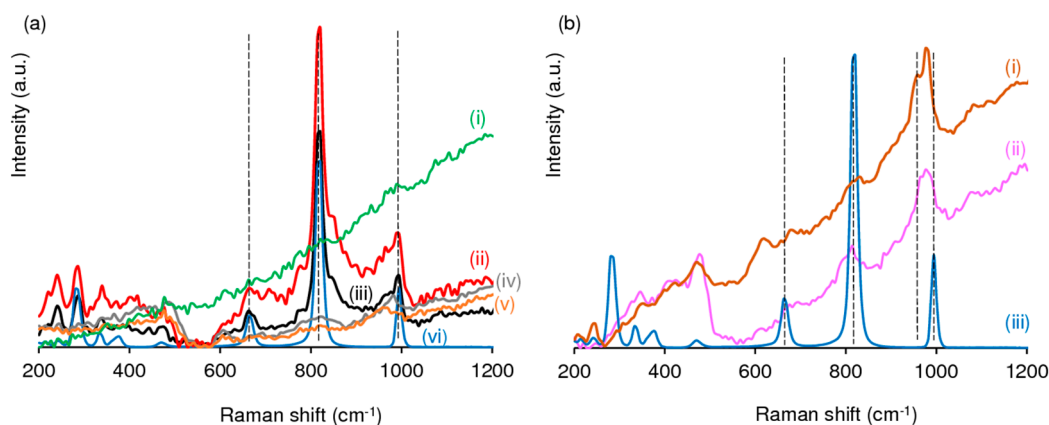


Figure 7. Raman spectra of (a) TUD-1(PT) ((i)-green), Mo-TUD(IWI-ahm) ((ii)-red), Mo-TUD(HT) ((iii)-black), Mo-TUD(IWI-acac) ((iv)-grey), Mo-TUD(IWI-amm) ((v)-orange), and bulk MoO₃ ((vi)-blue); and (b) Mo-hierBEA ((i)-brown), hierBEA ((ii)-pink) and bulk MoO₃ ((iii)-blue).

2.1.2. Hierarchical Micro-Mesoporous BEA Zeotype

The preparation and characterization of hierarchical micro-mesoporous hierBEA zeotype has already been reported by some of us [28]. Specifically, hierBEA was prepared via a top-down strategy involving desilication to form mesopores and dealumination to form reactive silanol nests for bonding transition metals to the framework [28]. The zeotype was essentially siliceous (Si/Al molar ratio = 697), microcrystalline, possessing both microporosity ($S_{\text{micro}} = 291 \text{ m}^2 \text{ g}^{-1}$; $V_{\text{micro}} = 0.12 \text{ cm}^3 \text{ g}^{-1}$) and mesoporosity ($S_{\text{meso}} = 468 \text{ m}^2 \text{ g}^{-1}$), and had no measurable Lewis or Brønsted acidity [28]. In the present work, hierBEA was subjected to solid state impregnation (SSI) of MoO₂(acac)₂ (denoted acac) and calcination, giving Mo-hierBEA. Since no wash/filtration steps were applied after SSI, the amount of molybdenum that was introduced during SSI ($0.21 \text{ mmol}_{\text{Mo}} \text{ g}^{-1}$, Si/Mo \cong 70) may remain in the final material.

The PXRD pattern of Mo-hierBEA showed the characteristic reflection peaks of isomorphous forms of zeolite Beta (main peaks at ca. 6.5–9 and 22.5° 2 θ , Figure 2), in agreement with those reported for hierBEA [28,43–45]; no peaks associated with other crystalline phases appeared. Hence, the BEA topology was essentially preserved during SSI/calcination, and did not possess Mo-containing crystallites. Elemental mappings showed uniformly distributed molybdenum (Figure 3c). The N₂ sorption isotherm of Mo-hierBEA was of type IV with a hysteresis loop associated with the mesoporosity (Figure 4b), similar to that reported for hierBEA [28]. Consistently, the pore size distributions of Mo-hierBEA included micropores (0.55–0.78 nm associated with the BEA topology; and 1.3–1.9 nm, which may correspond to larger pores formed via desilication) and mesopores (2.5–5 nm) (Figure 4b (inset), Table 1). The SSI process led essentially to a reduction of micropore surface area (Table 1), suggesting that at least a fraction of the Mo sites may be located inside micropores.

The ATR FT-IR spectra of Mo-hierBEA and hierBEA were similar, suggesting that the surface chemistry was preserved during SSI/calcination (Figure 5b). A very weak shoulder at ca. 925 cm⁻¹ may be due to surface oxomolybdenum sites (e.g., of tetrahedral {MoO₄} species) and/or Mo-O-Si bonds [46]. The DR UV-vis spectrum of the support hierBEA was featureless, whereas Mo-hierBEA exhibited overlapping bands at ca. 205, 250 and 300 nm (Figure 6), somewhat in parallel to that discussed above for the TUD-1 type materials. The Raman spectra of Mo-hierBEA and hierBEA were comparable, but the main difference was the appearance of a band at 958 cm⁻¹ for Mo-hierBEA, which did not appear for hierBEA (Figure 7). According to the literature, this band may be associated with well dispersed molybdenum species [39] and/or Si-O stretching of SiOH... OMo defective sites [16]. The spectral range 330–500 cm⁻¹ may have contributions from the O-Mo-O bending mode of surface Mo sites [13,41], and the band at 976 cm⁻¹ may have a

contribution from the stretching mode of the dioxomolybdenum moiety ($\text{Mo}(\text{=O})_2$) of $(\text{Si-O})_2\text{Mo}(\text{=O})_2$ type sites [7,13,16,41]. The bands associated with bulk MoO_3 were not clearly distinguished in the spectrum of Mo-hierBEA, supporting that this material possessed a relatively uniform distribution of molybdenum species.

2.2. Catalytic Studies

2.2.1. General Considerations

The TUD-1 type materials and the hierarchical zeotype Mo-hierBEA were first tested for the model reaction of *cis*-cyclooctene (Cy8) with TBHP (in decane), using α,α,α -trifluorotoluene (TFT) as a solvent, at 70 °C. Cyclooctene oxide (Cy8O) was the only product (100% selectivity) formed in quantitative yield within a 4–24 h reaction, depending on the type of catalyst and its preparation method. An exception was Mo-TUD(HT), for which quantitative epoxide yield was not reached within 24 h (although Cy8 selectivity was 100%). The carbon balances (based on the amount of olefin consumed and the amount of epoxide formed) closed in 100%. Without a catalyst, the Cy8 reaction was very sluggish (5% conversion at 24 h). Iodometric titrations (details in the experimental section) indicated that, in the presence of the molybdenum-containing catalysts, TBHP was efficiently consumed for olefin epoxidation, and no significant non-productive decomposition of TBHP (to O_2 plus *tert*-butanol) occurred.

Alternative oxidant solutions were tested, namely, aqueous solutions of TBHP (TBHPaq) and H_2O_2 . With these oxidant solutions, acetonitrile was used as solvent to avoid the formation of triphasic solid (catalyst)-liquid (aqueous)-liquid (organic) mixtures, which may suffer from severe mass transfer limitations. The use of TBHPaq or H_2O_2 had a detrimental effect on the catalytic reaction; e.g., for Mo-TUD(IWI-acac), Mo-hierBEA and Mo-TUD(HT), Cy8 conversion was less than 30% (100% Cy8O selectivity) at 4 h/70 °C (Figure 8). These results may be due to an interplay of several factors such as competitive sorption effects of the reactants versus water to the catalyst surface and/or in the coordination to the active sites. According to mechanistic studies reported in the literature, Mo-catalyzed epoxidation of olefins with hydroperoxide oxidants is generally a heterolytic mechanism where the oxidant molecules (Lewis base) coordinate to the metal center (Lewis acid), forming an oxidizing transition state responsible for (electrophilic) oxygen atom transfer to the olefin, finally giving the epoxide product plus the coproduct of the oxidant (i.e., *tert*-butanol for TBHP) [47–51]. Accordingly, water may have an inhibitory effect on the Lewis acid–base interactions. On the other hand, H_2O_2 may affect the catalyst stability [7].

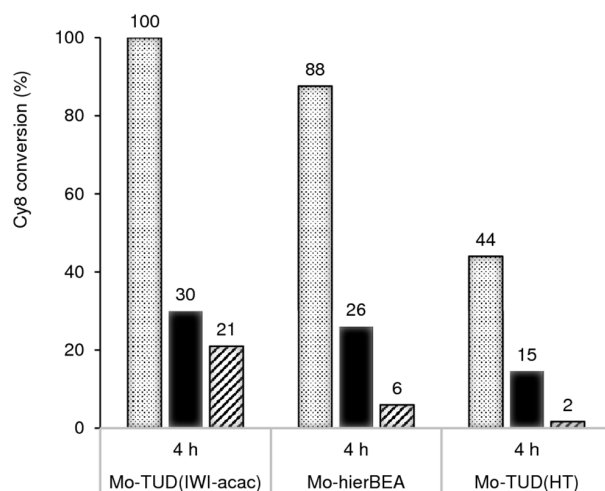


Figure 8. Influence of the type of oxidant solution on catalytic epoxidation of *cis*-cyclooctene (Cy8), at 70 °C (4 h), using the oxidant/solvent systems: TBHP in decane/TFT (dotted bars); TBHP in water/CH₃CN (black bars); H₂O₂ in water/CH₃CN (diagonally-striped bars). Epoxide selectivity was always 100%.

Based on the above results, the performances of the prepared catalysts were further studied using the organic solution of TBHP.

2.2.2. Mo-TUD(IWI) Type Catalysts

The Cy8/TBHP reaction in the presence of the Mo-TUD(IWI) type catalysts gave Cy8O as the only product (100% selectivity). Although these materials possessed the same Mo loading (Table 1), the reaction kinetics was different (Figure 9). The initial activity followed the order, Mo-TUD(IWI-acac) ($255 \text{ mmol}_{\text{Cy8}} \text{ g}_{\text{cat}}^{-1} \text{ h}^{-1}$) > Mo-TUD(IWI-amm) ($182 \text{ mmol}_{\text{Cy8}} \text{ g}_{\text{cat}}^{-1} \text{ h}^{-1}$) \gg Mo-TUD(IWI-ahm) ($79 \text{ mmol}_{\text{Cy8}} \text{ g}_{\text{cat}}^{-1} \text{ h}^{-1}$), and quantitative epoxide yield was reached at 4 h, 6 h and 24 h for Mo-TUD(IWI-acac), Mo-TUD(IWI-amm) and Mo-TUD(IWI-ahm), respectively. Based on the characterization studies, the Mo-TUD(IWI) materials may possess different distributions (type, concentration) of surface Mo species, which may partly explain the differences in activity; chemically different types of Mo sites may possess different intrinsic activities, affecting the catalytic performance. For example, based on the Raman studies, the least active catalyst Mo-TUD(IWI-ahm) seemed to possess relatively high nuclearity Mo species, which may have lower intrinsic activity. Somewhat supporting this hypothesis, a catalytic test using bulk MoO_3 as a catalyst led to 14%/37% conversion (100% Cy8O selectivity) at 6 h/24 h, 70 °C, which was much poorer than that for the Mo-TUD(IWI) type catalysts under similar reaction conditions (Figure 10).

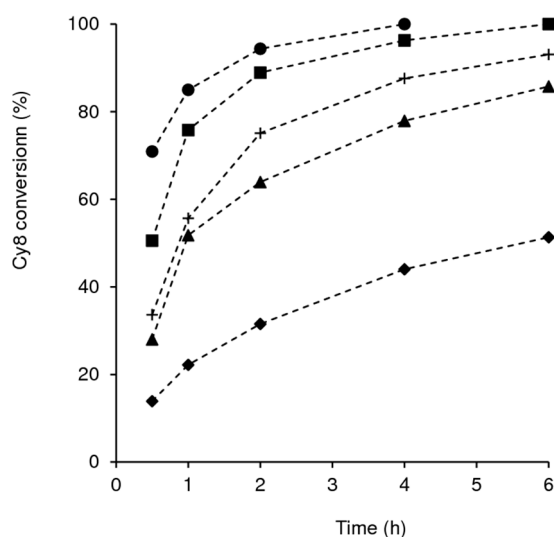


Figure 9. Kinetic profiles of the Cy8/TBHP reaction, in the presence of Mo-TUD(IWI-acac) (●), Mo-TUD(IWI-amm) (■), Mo-TUD(IWI-ahm) (▲), Mo-TUD(HT) (◆), or Mo-hierBEA (+), at 70 °C. Epoxide selectivity was always 100%.

For comparison, the free molybdenum precursor compounds ($\text{MoO}_2(\text{acac})_2$ (denoted acac), $(\text{NH}_4)_2\text{MoO}_4$ (denoted amm) and $(\text{NH}_4)_6\text{Mo}_7\text{O}_{24}$ (denoted ahm) that were used to prepare the Mo-TUD(IWI) materials, were tested as molecular catalysts (keeping constant the initial molar ratio Mo: Cy8:TBHP, as for the Mo-TUD(IWI) materials) (Figure 10). The three precursors led to Cy8O as the only product (100% selectivity). The precursors amm and ahm led to poor results (18% and 30% conversion at 6 h, respectively, Figure 10b,c), whereas precursor acac led to 100% conversion within 6 h (Figure 10a). These results may be partly due to differences in the Lewis acidity, solubility and/or stability of the free molybdenum compounds. For example, $\text{MoO}_2(\text{acac})_2$ was completely soluble in the olefin/solvent mixture, whereas $(\text{NH}_4)_2\text{MoO}_4$ and $(\text{NH}_4)_6\text{Mo}_7\text{O}_{24}$ were partially soluble. On the other hand, at 4 h, $(\text{NH}_4)_2\text{MoO}_4$ retained its original colour (white), $\text{MoO}_2(\text{acac})_2$ changed from orange to brown, and $(\text{NH}_4)_6\text{Mo}_7\text{O}_{24}$ changed from white to light yellow. Hence, the free molybdenum compounds in solution may suffer chemical modifications.

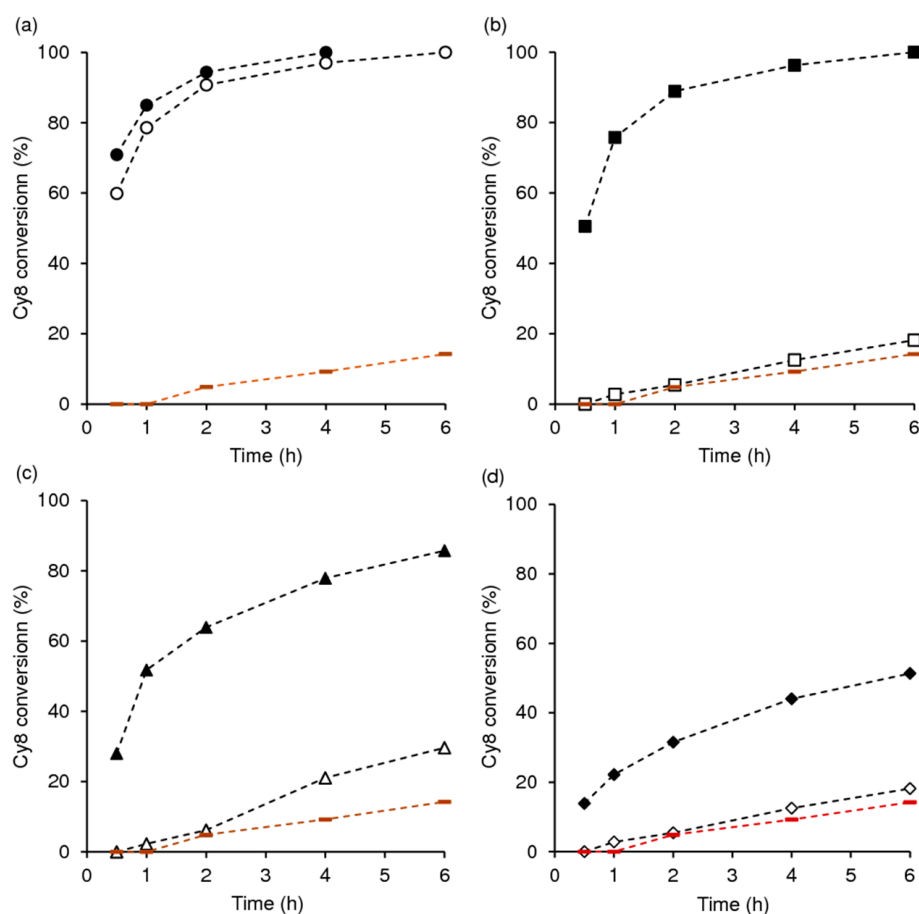


Figure 10. Comparison of the mesoporous silicates (solid symbols) to the respective molybdenum precursors (open symbols), for the epoxidation of *cis*-cyclooctene (Cy8) with TBHP at 70 °C: (a) Mo-TUD(IWI-acac) (●) and precursor acac (○); (b) Mo-TUD(IWI-amm) (■) and precursor amm (□); (c) Mo-TUD(IWI-ahm) (▲) and precursor ahm (△); and (d) Mo-TUD(HT) (◆) and precursor amm (◇). For comparison, results for bulk MoO₃ (-) are included in (a–d). Epoxide selectivity was always 100%.

To check the influence of the type of post-synthesis method (IWI versus SSI), the catalytic performances of Mo-TUD(IWI-acac) and Mo-TUD(SSI-acac) (possessing the same Mo loading, Table 1) were compared. Mo-TUD(SSI-acac) was less active than Mo-TUD(IWI-acac) (100% Cy8O selectivity for the two materials), suggesting that the IWI method was more effective for introducing active Mo species in TUD-1(PT) (Figure 11).

Comparisons of the catalytic results for the Mo-TUD(IWI) catalysts (2 wt% Mo; reaction conditions, 5.6 g_{cat}/mol_{Cy8}, TBHP: Cy8 = 1.5, 70 °C) with literature data for (fully inorganic) molybdenum impregnated on ordered mesoporous silica/silicates is not trivial due to the very different Cy8/TBHP reaction conditions used. For example, wet impregnation of a very high 45 wt% Mo loading on a mesoporous zirconium silicate led to 64% Cy8O selectivity at 38% Cy8 conversion after 8 h (using 50 g_{cat}/mol_{Cy8}; TBHP: Cy8 = 1; reflux, acetonitrile (b.p. = 82 °C) as solvent) [52]. Wet impregnation of molybdenum (ammonium molybdate precursor) on hollow mesoporous silica spheres (5 wt% Mo) led to 98% Cy8O selectivity at 91% Cy8 conversion, 4 h/80 °C (using 10 g_{cat}/mol_{Cy8}; TBHP: Cy8 = 2; 1,2-dichloroethane solvent) [53]. Molybdenum supported on hollow mesoporous silica spheres via wet impregnation/solvent evaporation/calcination (7 wt% MoO₃) led to 96% Cy8O selectivity at 99% Cy8 conversion, 2 h/80 °C, but using a very high amount of catalyst (75 g_{cat}/mol_{Cy8}; TBHP: Cy8 = 1.2; 1,2-dichloroethane solvent) [12].

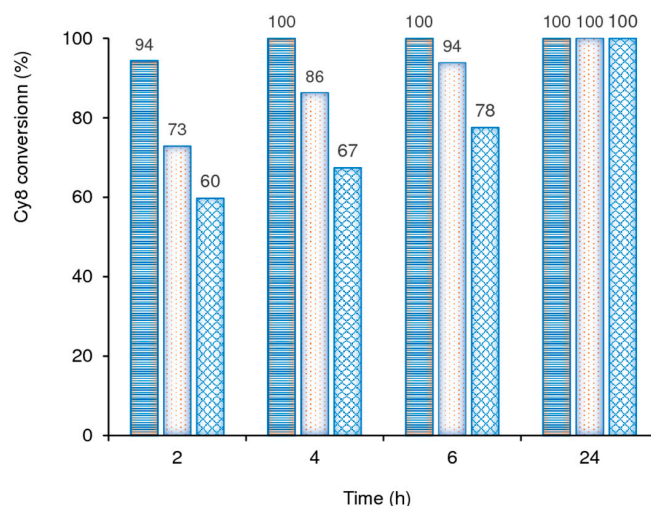


Figure 11. Influence of the post-synthesis IWI versus SSI methods, and the type of support (TUD-1 versus hierBEA) on the Cy8/TBHP reaction at 70 °C: Mo-TUD(IWI-acac) (horizontally-striped bars), Mo-TUD(SSI-acac) (dotted bars) or Mo-hierBEA (diamonds). Epoxide selectivity was always 100%.

2.2.3. Hydrothermal Synthesis Versus Post-Synthesis Strategies (TUD-1)

The hydrothermally synthesized (static conditions) material Mo-TUD(HT) was compared (on the same catalyst mass basis) with Mo-TUD(IWI-amm) prepared via post-synthesis IWI, using the same Mo precursor (amm). Mo-TUD(HT) led to 51%/86% Cy8 conversion at 6 h/24 h, 70 °C, and Cy8O was the only product (100% epoxide selectivity). Mo-TUD(HT) performed inferiorly to Mo-TUD(IWI-amm); initial catalytic activity was 50 and 182 $\text{mmol}_{\text{Cy8}} \text{g}_{\text{cat}}^{-1} \text{h}^{-1}$, and epoxide yield at 6 h was 51% and 100%, respectively (Figure 10b,d). These results may be partly due to differences in the Mo loading, which was lower for Mo-TUD(HT) (0.08 $\text{mmol}_{\text{Mo}} \text{g}^{-1}$ compared with 0.21 $\text{mmol}_{\text{Mo}} \text{g}^{-1}$ for Mo-TUD(IWI-amm), Table 1).

Comparison of the results for Mo-TUD(HT) (reaction conditions: 5.6 $\text{g}_{\text{cat}}/\text{mol}_{\text{Cy8}}$, TBHP: Cy8 = 1.5, 70 °C) with literature data for other hydrothermally synthesized fully inorganic molybdenum-containing ordered mesoporous silicas, tested as catalysts for Cy8/TBHP conversion, is difficult due to the very different reaction conditions used. For example, hydrothermally synthesized Mo-MCM-41 (4.21 wt% Mo; surfactant templating synthesis) and Mo-SBA-15 (2.35 wt% Mo: synthesis using a triblock copolymer P123) led to 97–99% conversion at 3 h/40 °C using a very high amount of catalyst (33.3 $\text{g}_{\text{cat}}/\text{mol}_{\text{Cy8}}$; TBHP: Cy8 = 3; decane as solvent) [16]. Hydrothermally synthesized bimetallic Mo-Ti-SBA-15 possessing a very high Mo loading (Si/Mo = 6.5) led to 98% Cy8O selectivity at 99% Cy8 conversion, 4 h/80 °C (using 10 $\text{g}_{\text{cat}}/\text{mol}_{\text{Cy8}}$, TBHP: Cy8 = 2; 1,2-dichloroethane as solvent) [54].

2.2.4. Hierarchical Mo-hierBEA

Hierarchical micro/mesoporous Mo-hierBEA led to 100% Cy8O selectivity at 93%/100% Cy8 conversion at 6 h/24 h and 70 °C (Figure 9). A material prepared via SSI of acac (keeping the Mo loading constant) on a commercial microcrystalline and microporous zeolite Beta, namely Mo-BEA, performed inferiorly; conversion at 4 h/6 h was 67%/78% for Mo-BEA and 88%/93% for Mo-hierBEA. Hence, the introduction of mesoporosity in the microporous zeolite considerably enhanced the catalytic activity.

To the best of our knowledge, no olefin epoxidation results were reported in the literature for fully inorganic Mo-containing intracrystalline hierarchical BEA zeotypes. Niederer and Hölderich [17] reported the synthesis of microporous Mo-containing H-[B]-BEA prepared via isomorphic substitution of B for Mo (Si/Mo \cong 37) which led to 28% Cy8O yield at 36% Cy8 conversion, 24 h/70 °C (chlorobenzene as solvent; TBHP: Cy8 = 0.5); the epoxide selectivity was 77%.

The catalytic performance of hierarchical Mo-hierBEA was compared with that of the ordered mesoporous materials Mo-TUD(IWI-acac) or Mo-TUD(SSI-acac) (Figure 11). Although the three materials were prepared via post-synthesis strategies using the acac precursor and the same Mo loading, Mo-hierBEA was less active. The characterization studies indicated that at least a fraction of Mo species may be located inside micropores (Table 1). These results, together with the fact that (i) the micropore sizes of BEA are ca. $7.6 \text{ \AA} \times 6.4 \text{ \AA}$ (linear channels) and ca. $5.5 \text{ \AA} \times 5.5 \text{ \AA}$ (tortuous channel), (ii) Cy8 molecules possess a molecular size of ca. 5.5 \AA [55,56], and (iii) both olefin and oxidant need to access the active sites to trigger epoxidation, suggest that the effective amount of active sites is possibly lower than the Mo loading.

2.2.5. Substrate Scope

The most active mesoporous catalyst Mo-TUD(IWI-acac) was tested with a broader substrate scope: 1-octene, *trans*-2-octene and the biomass-derived olefins *DL*-limonene and methyl oleate (TBHP, $70 \text{ }^\circ\text{C}$) (Figure 12). For Cy8, 1-octene, *trans*-2-octene and methyl oleate, the corresponding epoxide was the only product formed (100% epoxide selectivity). A comparison of the results for the terminal and internal linear C8 olefins indicated that *trans*-2-octene was more reactive than 1-octene. Based on the above mechanistic considerations, these results may be partly due to the higher electron density of the internal C=C bond of *trans*-2-octene, favoring the (electrophilic) atom transfer to the olefin. The higher reactivity of cyclic Cy8 than linear *trans*-2-octene suggests that epoxidation at endocyclic double bonds is favorable.

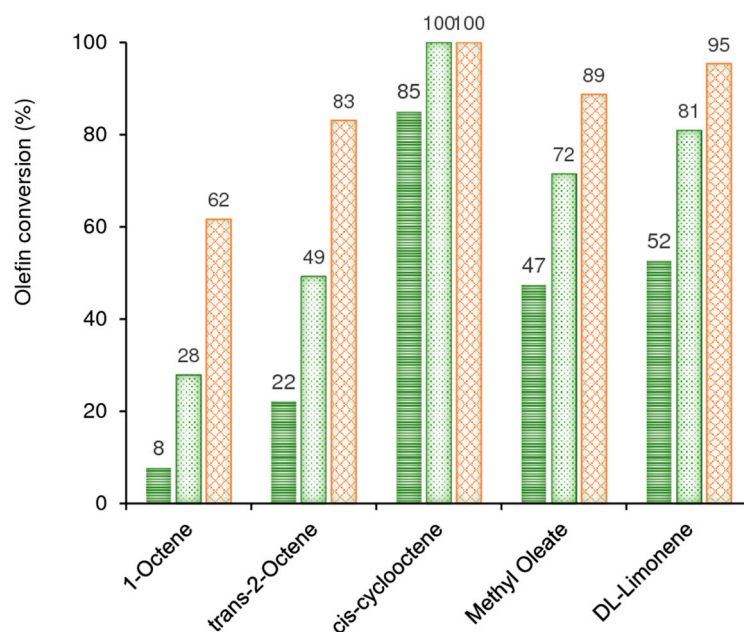


Figure 12. Olefin conversion at 1 h (horizontally-striped bars), 4 h (dotted bars) and 24 h (diamonds), in the presence of Mo-TUD(IWI-acac) (TBHP, $70 \text{ }^\circ\text{C}$). For all olefins excluding *DL*-limonene, epoxide selectivity was 100%.

The epoxidation of *DL*-limonene gave monoepoxide (1,2-epoxy-p-menth-8-ene) and diepoxide (1,2:8,9-diepoxyp-menthane) products in yields of 69% and 8%, respectively, at 4 h (81% conversion), and in yields of 57% and 15%, respectively, at 24 h (95% conversion). The drop of monoepoxide yield was approximately equal to the increment of diepoxide yield in the same time interval, indicating that the former is intermediate to the latter. These results, together with the fact that the main product was the monoepoxide, indicate high regioselectivity towards the epoxidation of the endocyclic C=C bond relative to the exocyclic one (consistent with the above mechanistic considerations).

Very few studies have been reported in the literature for the limonene/TBHP reaction in the presence of fully inorganic Mo-containing ordered mesoporous silicas. A study using hydrothermally synthesized Mo-MCM-41 (4.21 wt% Mo; synthesis via surfactant template route) and Mo-SBA-15 (2.35 wt% Mo; synthesis using polymer P123) reported 87% mono- and 9% diepoxide selectivity at 51% conversion, and 80% mono- and 14% diepoxide selectivity at 44% conversion, respectively, at 24 h and room temperature (pentane as solvent) [16]. In that study, a considerable amount of molybdenum catalyst relative to the substrate was used ($33.3 \text{ g}_{\text{cat}}/\text{mol}_{\text{olefin}}$ compared with $5.6 \text{ g}_{\text{cat}}/\text{mol}_{\text{olefin}}$ for Mo-TUD(IWI-acac)) and, on the other hand, TBHP:olefin was 2 compared with 1.5 for Mo-TUD(IWI-acac) [16]. An interesting study reported the continuous flow epoxidation reaction over Mo-MCM-41 (Si/Mo = 35; synthesized using the surfactant template route), which led to 96% epoxide selectivity at 80% (*R*)-(+)-limonene conversion, 24 h/20 °C (TBHP:olefin \cong 4; pentane as solvent; loss of activity occurred) [18].

The reaction of the fatty acid methyl ester, methyl oleate, in the presence of Mo-TUD(IWI-acac) at 70 °C, led to 100% selectivity towards the respective epoxidized product, namely, methyl 9,10-epoxystearate, which was formed in 72%/89% yield at 4 h/24 h (Figure 12). These results are relatively good, considering the literature data for the same catalytic reaction in the presence of fully inorganic Mo-containing ordered mesoporous silicates. A macro-mesoporous Mo-containing SBA-15 type material hydrothermally synthesized using several templates (Pluronic P123, poly(methyl methacrylate and cetyltrimethylammonium bromide) led to ca. 99% epoxide selectivity at 91% methyl oleate conversion, 11 h/80 °C (using $10 \text{ g}_{\text{cat}}/\text{mol}_{\text{olefin}}$; TBHP:olefin = 2; 1,2-dichloroethane as solvent); this material performed inferiorly to hydrothermally synthesized mesoporous Mo-SBA-15 [57]. Molybdenum supported on hollow mesoporous silica spheres (4.5 wt% MoO₃) led to 99% epoxide selectivity at 80%/100% conversion reached after 8 h/24 h at 80 °C (using a very high ratio $75 \text{ g}_{\text{cat}}/\text{mol}_{\text{Cy8}}$; TBHP:olefin = 1.2; 1,2-dichloroethane as solvent) [12].

2.2.6. Catalyst Stability

Hot filtration tests (details in the experimental section) were performed for each catalyst to check for leaching of active species. No significant increment of olefin conversion was verified for Mo-TUD(IWI-acac), Mo-TUD(IWI-amm) or Mo-hierBEA after separating the solid catalyst (Figure 13). Specifically, the increment of conversion until 6 h was 5–6%, which was similar to that for the blank test without a catalyst, suggesting the absence of soluble active species leached from these solid catalysts. Mo-TUD(IWI-ahm) led to a slightly higher increment in conversion (8%), and Mo-TUD(HT) led to a 15% increment in conversion, suggesting leaching of some active species for these two materials.

The catalysts were used for three consecutive batch runs of Cy8/TBHP reaction at 70 °C. Between runs, the materials were washed and dried. For all materials, a partial drop of catalytic activity occurred (Figure 14). For example, conversion at 6 h in run 3 followed the order: Mo-TUD(IWI-acac) (59%) > Mo-TUD(IWI-amm) (42%) > Mo-hierBEA (31%) > Mo-TUD(IWI-ahm) (24%) > Mo-TUD(HT) (7%); Cy8O selectivity was always 100%. For the three catalysts which led to the highest conversions in run 3, namely, Mo-TUD(IWI-acac), Mo-TUD(IWI-amm) and Mo-hierBEA, the Si/Mo ratios were comparable to those of the respective original materials: Si/Mo \cong 70 and 70 ± 8 for fresh and used Mo-TUD(IWI-acac), respectively; Si/Mo \cong 70 and 71 ± 4 for fresh and used Mo-TUD(IWI-amm), respectively; Si/Mo \cong 64 and 62 ± 8 for fresh and used Mo-hierBEA, respectively (EDS).

A possible catalyst deactivation phenomenon is the adsorption of organic matter on the catalyst surface during the catalytic reaction, which may passivate the active sites. However, calcination of the used catalyst Mo-TUD(IWI-acac) (500 °C, 1 °C/min, 3 h, under air), for example, led to a similar kinetic profile to that for the corresponding washed-dried catalyst (only slightly enhanced initial activity, Figure S2), suggesting that catalyst surface passivation by organic matter is not (at least solely) a factor responsible for catalyst deactivation.

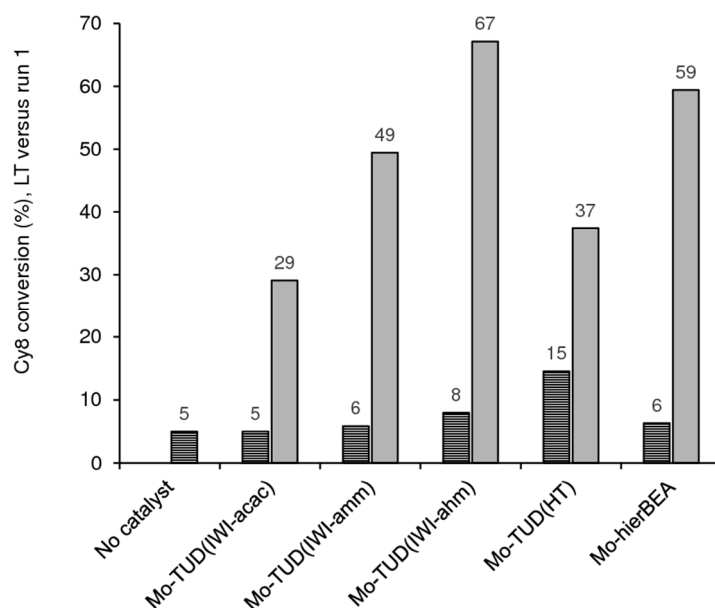


Figure 13. Increment of Cy8 conversion (between 30 min and 6 h, at 70 °C) for the leaching test (LT) (striped black bars), compared with the increment of conversion (in the same time interval) in the presence of solid catalyst (run 1; grey bars). The results for the reaction without catalyst are included.

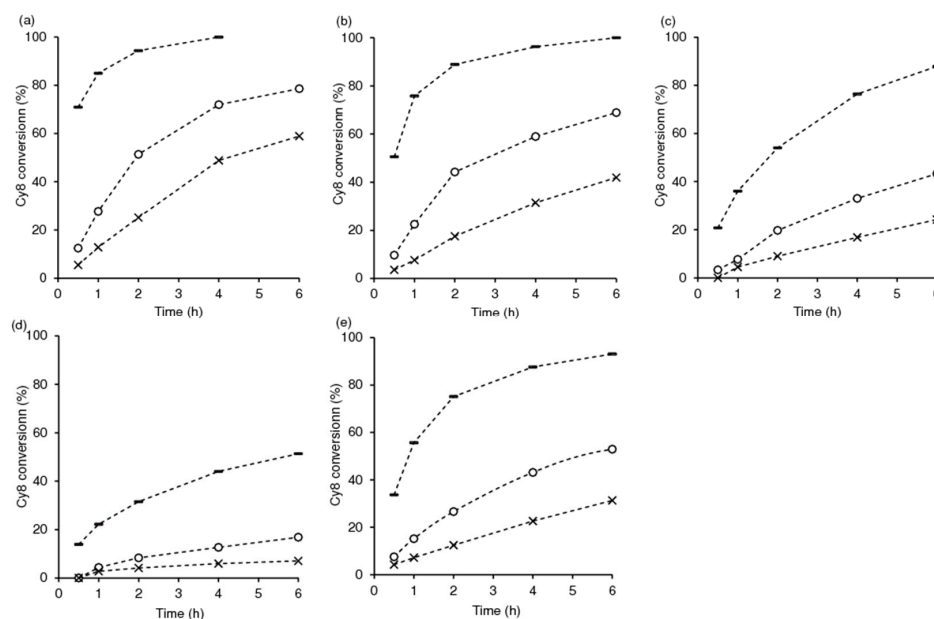


Figure 14. Consecutive batch runs (run 1 (-); run 2 (o); run 3 (×)) of Cy8/TBHP in the presence of (a) Mo-TUD(IWI-acac), (b) Mo-TUD(IWI-amm), (c) Mo-TUD(IWI-ahm), (d) Mo-TUD(HT) or (e) Mo-hierBEA, at 70 °C. Epoxide selectivity was always 100%.

Further characterization studies were carried out to study the catalyst deactivation phenomena. No significant differences between the original and used solids were verified based on the PXRD patterns (Figure S3a), morphology or metal distributions (exemplified in Figure S4) and ATR FT-IR spectra (Figure S3b). Strong fluorescence caused weak Raman spectra of the used TUD-1 type solids; on the other hand, for the original and used Mo-hierBEA catalyst, the spectral features were somewhat comparable (Figure S5). Nevertheless, one cannot rule out the possibility of a fraction of very active Mo sites undergoing chemical modifications in situ, giving less active or inactive Mo sites (although it was not possible to distinguish these differences by the above solid-state characterization techniques).

3. Materials and Methods

3.1. Materials

All chemicals were obtained from commercial sources (Sigma-Aldrich, Germany, unless indicated otherwise) and used as received. For syntheses, these included tetraethylorthosilicate (TEOS, 98%), triethanolamine (TEA, 97%, Fluka), tetraethylammonium hydroxide (TEAOH, 35% (w/w) aq.), ammonium heptamolybdate ((NH₄)₆Mo₇O₂₄, denoted ahm; 99%, Riedel-de-Haën), ammonium molybdate ((NH₄)₂MoO₄, denoted amm; 99.98%), bis(acetylacetonato)dioxomolybdenum(VI) (MoO₂(acac)₂, denoted acac; 100%), anhydrous absolute ethanol (EtOH, 99.9%, Carlo Erba), hydrogen peroxide (H₂O₂, 30% (w/w) aq.), hydrochloric acid (HCl, 37% aq., Panreac), deionized water (Milli-Q, Aldrich), and methanol (MeOH, >99.9%). For catalysis, the substrates included *cis*-cyclooctene (Cy8, 95%, Alfa Aesar), methyl oleate (99%), *DL*-limonene (>95%, Merck), 1-octene (98%), and *trans*-2-octene (97%); the oxidants were *tert*-butyl hydroperoxide (TBHP, in decane 5.5 M), aqueous *tert*-butyl hydroperoxide (TBHPaq, 70% (w/w) aq.) and aqueous hydrogen peroxide (H₂O₂, 30% (w/w) aq.); the solvents were anhydrous α,α,α -trifluorotoluene (TFT, \geq 99%), acetonitrile (99.9%, Panreac); the internal standards were undecane (\geq 99%) and methyl decanoate (99%). The support hierBEA corresponds to that reported in reference [28].

3.2. Synthesis of the Catalysts

3.2.1. Mo-TUD(IWI-x) Materials

Siliceous TUD-1 was prepared as described previously [58] and then subjected to a pretreatment (PT). For the pretreatment, a solution (80 mL) was prepared by mixing 79.7 mL 30% aq. H₂O₂ with 0.3 mL 37% aq. HCl, which was added to 1 g of TUD-1. After stirring for 1.5 h at 70 °C, the solid was separated by filtration, thoroughly washed with hot deionized water (ca. 60 °C) until neutral pH, and dried at 100 °C, giving powdered TUD-1(PT). Subsequently, TUD-1(PT) was subjected to incipient wetness impregnation (IWI) using different molybdenum precursors: MoO₂(acac)₂ (denoted acac), (NH₄)₂MoO₄ (denoted amm) and (NH₄)₆Mo₇O₂₄ (denoted ahm). Specifically, ca. 4.9 mL of 0.042 M Mo precursor solution was added slowly in a dropwise fashion to 1 g TUD-1-PT under mild stirring (ca. 500 rpm); the precursors amm and ahm were diluted in deionized water, and acac in methanol. The slurry was gently stirred at ambient temperature until the solid was dry. The resultant solid was calcined at 600 °C (heating rate of 1 °C min⁻¹) for 5 h, in air flow (20 mL min⁻¹), giving Mo-TUD(IWI-x), where x refers to the Mo precursor used (x = acac, amm or ahm).

For comparison, Mo-TUD(SSI-acac) was prepared in an identical fashion to that described in Section 3.2.3 for Mo-hierBEA, keeping the Mo loading (2 wt%) constant.

3.2.2. Mo-TUD(HT)

For comparative studies, Mo-TUD(HT) was synthesized via the sol-gel method, under hydrothermal (static) conditions (HT), as described in the literature [13]. Specifically, (NH₄)₂MoO₄ and TEOS were used as Mo and Si sources, respectively, and TEA and TEAOH were used as templating and mineralizing agents. The molar composition of the gel was 1SiO₂:xMoO_y:0.5TEAOH:1TEA:11H₂O. Specifically, (NH₄)₂MoO₄ (0.116 g) was added to TEA (5.5 mL) and deionized water (7.2 mL), giving mixture A. After stirring for 15 min, mixture A was added dropwise to TEOS (9.3 mL), under vigorous stirring, followed by dropwise addition of TEAOH (3 mL). This mixture was stirred for ca. 2.5 h at room temperature, subsequently aged for 24 h under static conditions, and then dried at 98 °C for 24 h. The solid was gently ground using an Agate mortar and pestle, and then hydrothermally treated in a 50 mL Teflon-lined stainless-steel autoclave for 24 h at 178 °C under autogenous pressure and static conditions. The resulting solid was subjected to Soxhlet extraction using ethanol for 4–6 h, dried overnight at 60 °C, gently ground using an Agate mortar and pestle, and finally calcined at 600 °C under air flow (20 mL min⁻¹) for 10 h (heating rate of 1 °C min⁻¹).

3.2.3. Mo-hierBEA

The previously reported hierarchical aluminosilicate zeotype hierBEA [28] was subjected to solid state impregnation (SSI) of $\text{MoO}_2(\text{acac})_2$. Specifically, hierBEA was mixed with $\text{MoO}_2(\text{acac})_2$ (in a total amount equivalent to $0.2 \text{ mmol}_{\text{Mo}} \text{ g}^{-1}$) and then gently ground using an Agate mortar and pestle (20 min mixing per 0.1 g of solid mixture). Finally, the solid was calcined at $550 \text{ }^\circ\text{C}$ ($1 \text{ }^\circ\text{C min}^{-1}$) for 5 h under air flow (20 mL min^{-1}), giving Mo-hierBEA.

3.3. Characterization of the Catalysts

The powder X-ray diffraction (PXRD) data were collected at room temperature on a Malvern Panalytical Empyrean diffractometer (Malvern Panalytical, Malvern, UK) equipped with a spinning flat sample holder and a PIXcel 1D detector set at 240 mm from the sample, in a Bragg-Brentano *para*-focusing optics configuration (45 kV, 40 mA). $\text{Cu-K}\alpha$ X-radiation ($\lambda_1 = 1.54060 \text{ \AA}$) filtered with a nickel foil was used. Samples were step-scanned from 3 to ca. 65° (2θ) in 0.026° steps with a counting time of 70 s per step.

EDS analysis and elemental (Mo, Si) mappings were obtained on a Hitachi SU-70 microscope (Hitachi High-Tech Europe GmbH, Krefeld, Germany) equipped with a Bruker Quantax 400 detector at 15 kV. Samples were prepared by deposition on aluminum sample holders followed by carbon coating using an Emitech K 950 carbon evaporator (Quorum Technologies, East Sussex, UK).

Nitrogen adsorption-desorption isotherms were measured at $-196 \text{ }^\circ\text{C}$ using a Quantachrome instrument (automated gas sorption data using Autosorb IQ2; Anton Paar Group, Florida, FL, USA). The samples were pretreated at $250 \text{ }^\circ\text{C}$ for 3 h under vacuum ($<4 \times 10^{-3}$ bar). The total specific surface area was calculated using the Brunauer, Emmett, Teller equation (S_{BET}), the total pore volume (V_p) was based on the Gurvitch rule (for a relative pressure (p/p_0) of at least 0.99), and the mesopore surface area (S_{meso}) and micropore volume (V_{micro}) were calculated using the *t*-plot method. The pore size distributions were calculated by the DFT method (adsorption branch).

For semi-quantitative comparison of the concentration of surface silanol groups of TUD-1 and TUD-1(PT), thermogravimetric (TGA) measurements were carried out on a Hitachi STA300 (Hitachi High-Tech Europe GmbH, Krefeld, Germany) device by heating the samples to $800 \text{ }^\circ\text{C}$ (heating rate of $10 \text{ }^\circ\text{C min}^{-1}$) under nitrogen flow (20 mL min^{-1}). Following similar procedures to those described in the literature for silicas [59], the concentration of surface silanol groups ($\text{mmol}_{\text{SiOH}} \text{ g}^{-1}$) was calculated based on the mass loss in the temperature range $180\text{--}650 \text{ }^\circ\text{C}$ (Δm , expressed in g) using the following equation: $\text{mmol}_{\text{SiOH}} \text{ g}^{-1} = [2 \times 1000 \times \Delta m / (M_{\text{H}_2\text{O}} \times m_i)]$, where $M_{\text{H}_2\text{O}}$ is the molar mass of water (18 g mol^{-1}) and m_i is the initial mass of sample (expressed in g).

ICP-OES analysis (for Si and Mo) was carried out on a Horiba JobinYvon Activa M spectrometer (HORIBA Jobin Yvon Inc., Edison, NJ, USA; detection limit of ca. $20 \text{ } \mu\text{g dm}^{-3}$; experimental range of error of ca. 5%); prior to analysis, 10 mg of solid sample was digested using 1 mL HF and 1 mL HNO_3 , and microwave heating at $180 \text{ }^\circ\text{C}$.

Attenuated total reflectance (ATR) FT-IR spectra were measured on a Bruker Tensor 27 spectrometer (Bruker, Billerica, MA, USA) equipped with a Specac Golden Gate Mk II ATR accessory (Specac, Orpington, UK) with a diamond top plate and KRS-5 focusing lenses (resolution 4 cm^{-1} , 256 scans). Diffuse reflectance UV-vis spectra were recorded on a Jasco V-780 spectrophotometer (Jasco Europe, Cremella, Italy) using an integrating sphere coated with barium sulfate with light detection by a built-in photomultiplier tube attached to the base of the sphere in reflectance mode with a wavelength scan speed of 200 nm min^{-1} in the range $190\text{--}900 \text{ nm}$, step size of 0.5 nm , and a slit width of 2.0 nm .

The Raman acquisitions were undertaken using a compact Raman 532 ER instrument (Wasatch Photonics, Morrisville, PA, USA) installed in a metallurgical microscope (Olympus BH2), enabling the micro-Raman back-scattering mode (532 nm laser line, $20\text{--}80 \text{ mW}$ laser power, 20 s integration time, $15 \text{ } \mu\text{m}$ spot size diameter).

3.4. Catalytic Tests

The catalytic epoxidation of olefins (1.8 mmol) with TBHP (2.75 mmol) was carried out at 70 °C in the presence of 10 mg of catalyst, using α,α,α -trifluorotoluene (TFT) as solvent (1 mL). The free molybdenum precursor compounds were tested with *cis*-cyclooctene (Cy8) as substrate under similar conditions (1.8 mmol Cy8, 2.75 mmol TBHP, 2.1 μ mol Mo, 70 °C). The catalyst, substrate and solvent were added to a 10 mL capacity borosilicate batch reactor equipped with a magnetic stirring bar (1000 rpm, optimized to avoid external mass transfer limitations). The loaded reactor was closed and immersed in a thermostatically controlled (and stirred) oil bath. After preheating the loaded reactor for 10 min, the oxidant (also preheated at 70 °C) was added to the reactor; this instant was considered as the initial instant of the catalytic reaction (the preheating operations warranted isothermal conditions from the initial instant). The evolution of the reactions was monitored by analyzing freshly prepared samples by gas chromatography (GC) using a Varian 450 GC instrument equipped with a BR-5 capillary column (30 m \times 0.25 mm \times 0.25 μ m; H₂ as carrier gas) and FID detector. The quantifications of reactants and products were based on calibrations using an internal standard (undecane for all substrates, excluding methyl oleate for which methyl decanoate was used).

After the catalytic reaction, the solid catalyst was separated by centrifugation (3500 rpm), thoroughly washed with acetone, dried overnight under atmospheric conditions, and finally vacuum-dried (ca. 0.1 bar) at 60 °C for at least 1 h. The recovered catalysts were reused, keeping the initial mass ratio catalyst:olefin:oxidant constant in consecutive batch runs. The leaching tests (LT) were carried out as follows: after 30 min of the Cy8/TBHP reaction in the presence of solid catalyst, the latter was separated from the reaction mixture at the reaction temperature (70 °C) using a 0.2 μ m PTFE membrane filter; the filtrate (solution) was transferred to a separate pre-heated (clean) reactor and stirred for a further 6 h at 70 °C; the reaction in the homogeneous phase was monitored by GC (an increment in Cy8 conversion indicates that active soluble species were leached from the solid catalyst into the liquid phase prior to the catalyst filtration step).

The consumption of TBHP was measured by iodometric titration. Specifically, the reactor containing the catalyst, solvent and oxidant was heated at 70 °C for 4 h. After cooling the reactor to ambient temperature and centrifugation (3500 rpm), samples were withdrawn for titration. The non-productive oxidant decomposition (into O₂) was calculated as the difference between the initial and final concentration of the oxidant.

4. Conclusions

Fully inorganic mesostructured TUD-1 type materials and a hierarchical (micro/mesoporous) BEA zeotype were used as supports for introducing molybdenum via different methodologies, and their catalytic performances (after calcination) were studied for the liquid phase epoxidation of relatively bulky C8 olefins and bio-based methyl oleate and *DL*-limonene, using *tert*-butyl hydroperoxide (TBHP) as oxidant, at 70 °C. Preliminary catalytic epoxidation studies indicated that an organic solution of TBHP was a far more effective oxidant solution than aqueous TBHP or H₂O₂.

The methodology used for the post-synthesis introduction of Mo species (incipient wetness impregnation (IWI) versus solid-state impregnation (SSI)) on a pre-treated TUD-1(PT) support, as well as the type of Mo precursor compound (acac, amm, ahm), influenced the material's surface chemistry and, consequently, the catalytic activity (based on the model reaction of *cis*-cyclooctene (Cy8) with TBHP); epoxide (Cy8O) selectivity was always 100%. The characterization studies suggested that the IWI method and the use of the mononuclear acac and amm precursors seemed to favor the formation of lower nuclearity molybdenum surface species and led to superior catalytic activity.

In comparison with the post-synthesis strategies, the (one-pot) hydrothermal synthesis of Mo-TUD(HT) (under static conditions using the same Si/Mo ratio in the synthesis gel as that used in the post-synthesis strategies) led to lower Mo loading in the final material (i.e., a fraction of the Mo of the synthesis gel was not introduced in the final material), which partly

contributed to a slower Cy8 epoxidation reaction. Hence, the post-synthesis strategies may allow a better control over the metal loading and enhanced olefin reaction kinetics.

The hierarchical hierBEA zeotype support was effective for introducing relatively well dispersed molybdenum species via SSI (using the acac precursor). The SSI method is a simple, neat strategy and advantageously avoids the use of solvents and downstream solvent separation processes. However, Mo-hierBEA was less active than its counterparts Mo-TUD(IWI-acac) and Mo-TUD(SSI-acac), which may be partly due to some active sites of Mo-hierBEA, particularly those located inside micropores, being less accessible to the relatively bulky reactant molecules.

The most active mesoporous catalyst Mo-TUD(IWI-acac) effectively promoted the epoxidation of linear (1-octene, *trans*-2-octene) and biobased olefins (methyl oleate, *DL*-limonene) at 70 °C. *DL*-limonene was converted to the corresponding mono- and diepoxide products in 69% and 8% yields, respectively, at 81% conversion (4 h). On the other hand, methyl oleate was converted to the epoxide in 100% selectivity at 89% conversion (24 h).

Catalytic stability studies carried out for three representative materials of the catalyst preparation strategies used (Mo-TUD(IWI-acac), Mo-hierBEA, and Mo-TUD(HT)), suggested the inexistence of measurable catalytic contributions from soluble metal species, albeit partial loss of activity in consecutive batch runs occurred. The solid-state characterization studies of the used materials did not reveal significant differences between the fresh and used solids. However, one cannot exclude the possibility of a fraction of relatively active Mo-sites suffering chemical changes under the catalytic reaction conditions, forming less active or inactive sites. Future in situ characterization studies under the catalytic reaction conditions and/or more detailed molecular-level surface characterization studies may valuably contribute to a better understanding of the catalyst deactivation phenomena and the improvement and development of more efficient catalyst preparation strategies.

Supplementary Materials: The following supporting information can be downloaded at: <https://www.mdpi.com/article/10.3390/catal12121513/s1>, Figure S1: PXRD pattern (a) and N₂ sorption isotherms (b) (inset shows the pore size distribution) of Mo-TUD(SSI-acac); Figure S2: Kinetic profiles for Mo-TUD(IWI-acac) used after wash-dry processes (●) or calcination (■) in batch run 2 of the Cy8/TBHP reaction, at 70 °C; Figure S3: PXRD patterns (a) and ATR FT-IR spectra (b) of fresh (i) and used (ii) Mo-hierBEA; fresh (iii) and used (iv) Mo-TUD(IWI-acac); fresh (v) and used (f) Mo-TUD(HT); Figure S4: SEM images and elemental (Si (green); Mo (red)) mappings of fresh (a) and used (b) Mo-TUD(HT), and fresh (c) and used (d) Mo-hierBEA; Figure S5: Raman spectra of fresh (a) and used (b) Mo-hierBEA.

Author Contributions: D.M.G.: data curation, formal analysis, investigation, writing—original draft preparation, validation, visualization, editing. P.N.: formal analysis, investigation, methodology, validation, visualization, project administration, supervision. M.M.A.: data curation, formal analysis, validation, visualization. A.J.S.F.: data curation, formal analysis. M.P.: visualization, resources, funding acquisition. A.A.V.: methodology, conceptualization, visualization, writing—review and editing, funding acquisition, supervision. All authors have read and agreed to the published version of the manuscript.

Funding: This work was developed within the scope of the project CICECO-Aveiro Institute of Materials, UIDB/50011/2020, UIDP/50011/2020 & LA/P/0006/2020, financed by national funds through the FCT/MEC (PIDDAC), and by Project POCI-01-0145-FEDER-030075 (COMPETE 2020 Operational Thematic Program for Competitiveness and Internationalization), co-financed by national funds through the FCT/MCTES and the European Union through the European Regional Development Fund under the Portugal 2020 Partnership Agreement. D.M.G. (grant ref. 2021.04756.BD) acknowledges the FCT for PhD grant (State Budget, European Social Fund (ESF) within the framework of Portugal 2020, namely through the Centro 2020 Regional Operational Program). The position held by MMA was funded by national funds (OE) through FCT, IP, in the scope of the framework contract foreseen in the numbers 4, 5 and 6 of article 23 of the Decree-Law 57/2016 of 29 August, changed by Law 57/2017 of 19 July.

Data Availability Statement: The original contributions presented in the study are included in the article/Supplementary Material and further inquiries can be directed to the corresponding authors.

Acknowledgments: The authors are grateful to Rosário Soares from the Department of Chemistry, CICECO-Aveiro Institute of Materials (University of Aveiro) for the assistance with PXRD data.

Conflicts of Interest: The authors declare no conflict of interest.

References

1. Bakhtyari, A.; Makarem, M.A.; Rahimpour, M.R. Light Olefins/Bio-Gasoline Production from Biomass. In *Bioenergy Systems for the Future*; Elsevier: Amsterdam, The Netherlands, 2017; pp. 87–148. [CrossRef]
2. Nijhuis, T.A.; Makkee, M.; Moulijn, J.A.; Weckhuysen, B.M. The Production of Propene Oxide: Catalytic Processes and Recent Developments. *Ind. Eng. Chem. Res.* **2006**, *45*, 3447–3459. [CrossRef]
3. Tert-Butyl Hydroperoxide | Ataman Kimya A.Ş. Available online: <https://www.ataman-Chemicals.com/en/products/tert-butyl-hydroperoxide-1817.html> (accessed on 22 October 2022).
4. Brégeault, J.M. Transition-Metal Complexes for Liquid-Phase Catalytic Oxidation: Some Aspects of Industrial Reactions and of Emerging Technologies. *J. Chem. Soc. Dalton Trans.* **2003**, *3*, 3289–3302. [CrossRef]
5. Smith, M.B. Functional Group Exchange Reactions: Oxidations. In *Organic Synthesis*; Elsevier (Academic Press): London, UK, 2017. [CrossRef]
6. Serge Hub, V.; Philippe Maj, B. Manufacture of Tertibutyl Hydroperoxide from Renewable Materials, Tertibutyl Hydroperoxide Thus Obtained, and Used Thereof. U.S. Patent US8536379B2, 17 September 2013. Available online: <https://patents.google.com/patent/US8536379B2/en> (accessed on 22 October 2022).
7. Ayla, E.Z.; Potts, D.S.; Bregante, D.T.; Flaherty, D.W. Alkene Epoxidations with H₂O₂ over Groups 4–6, Metal-Substituted BEA Zeolites: Reactive Intermediates, Reaction Pathways, and Linear Free-Energy Relationships. *ACS Catal.* **2021**, *11*, 139–154. [CrossRef]
8. Juwiler, D.; Blum, J.; Neumann, R. Metal Silicates by a Molecular Route as Catalysts for Epoxidation of Alkenes with tert-Butyl Hydroperoxide. *Chem. Commun.* **1998**, *10*, 1123–1124. [CrossRef]
9. Dusi, M.; Mallat, T.; Baiker, A. Epoxidation of Functionalized Olefins over Solid Catalysts. *Catal. Rev.-Sci. Eng.* **2000**, *42*, 213–278. [CrossRef]
10. Shen, Y.; Jiang, P.; Wai, P.T.; Gu, Q.; Zhang, W. Recent Progress in Application of Molybdenum-Based Catalysts for Epoxidation of Alkenes. *Catalysts* **2019**, *9*, 31. [CrossRef]
11. Wang, B.; Guo, T.; Peng, X.; Chen, F.; Lin, M.; Xia, C.; Zhu, B.; Liao, W.; Luo, Y.; Shu, X. Molybdenum-Confined Hierarchical Titanium Silicalite-1: The Synthesis, Characterization, and Catalytic Activity in Alkene Oxidation. *Ind. Eng. Chem. Res.* **2020**, *59*, 1093–1100. [CrossRef]
12. Kuwahara, Y.; Furuichi, N.; Seki, H.; Yamashita, H. One-Pot Synthesis of Molybdenum Oxide Nanoparticles Encapsulated in Hollow Silica Spheres: An Efficient and Reusable Catalyst for Epoxidation of Olefins. *J. Mater. Chem. A* **2017**, *5*, 18518–18526. [CrossRef]
13. Hamdy, M.S.; Mul, G. Synthesis, Characterization and Catalytic Performance of Mo-TUD-1 Catalysts in Epoxidation of Cyclohexene. *Catal. Sci. Technol.* **2012**, *2*, 1894–1900. [CrossRef]
14. Adam, F.; Iqbal, A. Silica Supported Amorphous Molybdenum Catalysts Prepared via Sol-Gel Method and Its Catalytic Activity. *Microporous Mesoporous Mater.* **2011**, *141*, 119–127. [CrossRef]
15. Bakala, P.C.; Briot, E.; Piquemal, J.Y.; Brégeault, J.M.; Beaunier, P. Comparison of the Conventional Impregnation Method Using Ammonium Heptamolybdate with a Simple Route to Silica-Supported Molybdenum(VI) Materials. *Catal. Commun.* **2007**, *8*, 1447–1451. [CrossRef]
16. Bakala, P.C.; Briot, E.; Salles, L.; Brégeault, J.M. Comparison of Liquid-Phase Olefin Epoxidation over MoO_x Inserted within Mesoporous Silica (MCM-41, SBA-15) and Grafted onto Silica. *Appl. Catal. A Gen.* **2006**, *300*, 91–99. [CrossRef]
17. Niederer, J.P.M.; Hölderich, W.F. Oxidation Capabilities of BEA Isomorphously Substituted with Molybdenum, Vanadium and Titanium: An Explorative Study. *Appl. Catal. A Gen.* **2002**, *229*, 51–64. [CrossRef]
18. Piquemal, J.Y.; Manoli, J.M.; Beaunier, P.; Ensuque, A.; Tougne, P.; Legrand, A.P.; Brégeault, J.M. Using Inorganic Silicate Precursor/Molybdenum Peroxo Complexes/Onium Salt Interfaces in Aqueous Acidic Media to Design Mesoporous Silica with High Molybdenum Content and High Dispersion. *Microporous Mesoporous Mater.* **1999**, *29*, 291–304. [CrossRef]
19. Telalovi, S. TUD-1: Synthesis and Application of a Versatile Catalyst, Carrier, Material. *J. Mater. Chem.* **2010**, *20*, 642–658. [CrossRef]
20. Angevine, P.J.; Gaffney, A.M.; Shan, Z.; Koegler, J.H.; Yeh, C.Y. TUD-1: A Generalised Mesoporous Catalyst Family for Industrial Applications. In Proceedings of the 235th ACS National Meeting, New Orleans, LA, USA, 6–10 April 2008.
21. Ooi, Y.K.; Hussin, F.; Yuliati, L.; Lee, S.L. Comparison Study on Molybdena-Titania Supported on TUD-1 and TUD-C Synthesized via Sol-Gel Templating Method: Properties and Catalytic Performance in Olefins Epoxidation. *Mater. Res. Express* **2019**, *6*, 074001. [CrossRef]

22. Ooi, Y.K.; Yuliati, L.; Hartanto, D.; Nur, H.; Lee, S.L. Mesostructured TUD-C Supported Molybdena Doped Titania as High Selective Oxidative Catalyst for Olefins Epoxidation at Ambient Condition. *Microporous Mesoporous Mater.* **2016**, *225*, 411–420. [[CrossRef](#)]
23. Sato, T.; Dakka, J.; Sheldon, R.A. Titanium-Substituted Zeolite Beta(Ti-Al- β)-Catalysed Epoxidation of Oct-1-ene with tert-Butyl Hydroperoxide (TBHP). *J. Chem. Soc. Chem. Commun.* **1994**, *16*, 1887–1888. [[CrossRef](#)]
24. Corma, A.; Esteve, P.; Martinez, A.; Valencia, S. Oxidation of Olefins with Hydrogen Peroxide and Tert-Butyl Hydroperoxide on Ti-Beta Catalyst. *J. Catal.* **1995**, *152*, 18–24. [[CrossRef](#)]
25. Sheldon, R.A.; Arends, I.W.C.E.; Lempers, H.E.B. Activities and Stabilities of Redox Molecular Sieve Catalysts in Liquid Phase Oxidations. A Review. *Collect. Czech. Chem. Commun.* **1998**, *63*, 1724–1742. [[CrossRef](#)]
26. Sotomayor, F.J.; Cychosz, K.A.; Thommes, M.; Sotomayor, F.; Cychosz, K.A.; Thommes, M. Characterization of Micro/Mesoporous Materials by Physisorption: Concepts and Case Studies. *Acc. Mater. Surf. Res.* **2018**, *3*, 34–50.
27. Schlumberger, C.; Thommes, M. Characterization of Hierarchically Ordered Porous Materials by Physisorption and Mercury Porosimetry—A Tutorial Review. *Adv. Mater. Interfaces* **2021**, *8*, 2002181. [[CrossRef](#)]
28. Antunes, M.M.; Silva, A.F.; Fernandes, A.; Pillinger, M.; Ribeiro, F.; Valente, A.A. Renewable Bio-Based Routes to γ -Valerolactone in the Presence of Hafnium Nanocrystalline or Hierarchical Microcrystalline Zeotype Catalysts. *J. Catal.* **2022**, *406*, 56–71. [[CrossRef](#)]
29. Mehmood, Y.; Khan, I.U.; Shahzad, Y.; Khalid, S.H.; Yousaf, A.M.; Hussain, T. Facile Synthesis of Mesoporous Silica Nanoparticles Using Modified Sol- Gel Method: Optimization and in Vitro Cytotoxicity Studies. *Pak. J. Pharm. Sci.* **2019**, *32*, 1805–1812. [[PubMed](#)]
30. Shawky, S.M.; Abo-ahassan, A.A.; Lill, H.; Bald, D.; El-khamisy, S.F.; Ebeid, E.M. Efficient Loading and Encapsulation of Anti-Tuberculosis Drugs Using Multifunctional Mesoporous Silicate Nanoparticles Running Title: Mesoporous Silicate Nanoparticles as Smart Drug Delivery System. *J. Nanosci. Curr. Res.* **2016**, *1*, 1–8. [[CrossRef](#)]
31. Ayu, G.; Kusumah, P.; Azizah, M. Silica Content and Structure from Corncob Ash with Various Acid Treatment (HCl, HBr, and Citric Acid). *Molekul* **2017**, *12*, 174–181. [[CrossRef](#)]
32. Gu, Q.; Jiang, P.P.; Shen, Y.; Zhang, K.; Wai, P.T.; Haryono, A. High-Dispersed MoO₃ Nanoparticles in 3D-Dendritic Mesoporous Silica Nanospheres: Heterogeneous Catalysts for the Epoxidation of Olefins. *J. Porous Mater.* **2021**, *28*, 779–789. [[CrossRef](#)]
33. Uchagawkar, A.; Ramanathan, A.; Hu, Y.; Subramaniam, B. Highly Dispersed Molybdenum Containing Mesoporous Silicate (Mo-TUD-1) for Olefin Metathesis. *Catal. Today* **2020**, *343*, 215–225. [[CrossRef](#)]
34. Hahn, T.; Bentrup, U.; Armbrüster, M.; Kondratenko, E.V.; Linke, D. The Enhancing Effect of Brønsted Acidity of Supported MoOx Species on Their Activity and Selectivity in Ethylene/Trans-2-Butene Metathesis. *ChemCatChem* **2014**, *6*, 1664–1672. [[CrossRef](#)]
35. Thielemann, J.P.; Ressler, T.; Walter, A.; Tzolova-müller, G.; Hess, C. Applied Catalysis A: General Structure of Molybdenum Oxide Supported on Silica SBA-15 Studied by Raman, UV-Vis and X-Ray Absorption Spectroscopy. *Appl. Catal. A Gen.* **2011**, *399*, 28–34. [[CrossRef](#)]
36. Song, Z.; Mimura, N.; Bravo-Suárez, J.J.; Akita, T.; Tsubota, S.; Oyama, S.T. Gas-Phase Epoxidation of Propylene through Radicals Generated by Silica-Supported Molybdenum Oxide. *Appl. Catal. A Gen.* **2007**, *316*, 142–151. [[CrossRef](#)]
37. Ramanathan, A.; Wu, J.; Maheswari, R.; Hu, Y. Microporous and Mesoporous Materials Synthesis of Molybdenum-Incorporated Mesoporous Silicates by Evaporation-Induced Self-Assembly: Insights into Surface Oxide Species and Corresponding Olefin Metathesis Activity. *Microporous Mesoporous Mater.* **2017**, *245*, 118–125. [[CrossRef](#)]
38. Ding, K.; Gulec, A.; Johnson, A.M.; Drake, T.L.; Wu, W.; Lin, Y.; Weitz, E.; Marks, L.D.; Stair, P.C. Highly Efficient Activation, Regeneration, and Active Site Identification of Oxide-Based Olefin Metathesis Catalysts. *ACS Catal.* **2016**, *5*, 5740–5746. [[CrossRef](#)]
39. Chandra, P.; Doke, D.S.; Umbarkar, B.; Biradar, A.V. One-Pot Synthesis of Ultrasmall MoO₃. *J. Mater. Chem. A* **2014**, *2*, 19060–19066. [[CrossRef](#)]
40. Chen, C.; Cai, L.; Zhang, L.; Fu, W.; Hong, Y.; Gao, X.; Jiang, Y.; Li, L. Transesterification of Rice Bran Oil to Biodiesel Using Mesoporous NaBeta Zeolite-Supported Molybdenum Catalyst: Experimental and Kinetic Studies. *Chem. Eng. J.* **2020**, *382*, 122839. [[CrossRef](#)]
41. Tian, H.; Roberts, C.A.; Wachs, I.E. Molecular Structural Determination of Molybdena in Different Environments: Aqueous Solutions, Bulk Mixed Oxides, and Supported MoO₃ Catalysts. *J. Phys. Chem. C* **2010**, *114*, 14110–14120. [[CrossRef](#)]
42. Lee, E.L.; Wachs, I.E. In Situ Spectroscopic Investigation of the Molecular and Electronic Structures of SiO₂ Supported Surface Metal Oxides. *J. Phys. Chem. C* **2007**, *111*, 14410–14425. [[CrossRef](#)]
43. Higgins, J.B.; La Pierre, R.B.; Schlenker, J.L.; Rohrman, A.C.; Wood, J.D.; Ker, G.T.; Rohrbaugh, W.J. The framework topology of zeolite beta. *Zeolites* **1988**, *8*, 446–452. [[CrossRef](#)]
44. Hajjar, R.; Millot, Y.; Man, P.P.; Che, M.; Dzwigaj, S.J. Two Kinds of Framework Al Sites Studied in BEA Zeolite by X-ray Diffraction, Fourier Transform Infrared Spectroscopy, NMR Techniques, and V Probe. *Phys. Chem. C* **2008**, *112*, 20167–20175. [[CrossRef](#)]
45. Costa, D.G.; Capaz, R.B. Structural analysis of zeolite beta through periodic ab initio simulations of XRD and ²⁹Si and ¹⁷O NMR spectra. *J. Mol. Struct.* **2015**, *1097*, 112–116. [[CrossRef](#)]
46. Li, C.; Xin, Q.; Wang, K.-L.; Gu, X. FT-IR Emission Spectroscopy Studies of Molybdenum Oxide and Supported Molybdena on Alumina, Silica, Zirconia, and Titania. *Appl. Spectrosc.* **1991**, *45*, 874–882. [[CrossRef](#)]
47. Veiros, L.F.; Prazeres, A.; Costa, P.J.; Romão, C.C.; Kühn, F.E.; José Calhorda, M. Olefin Epoxidation with Tert-Butyl Hydroperoxide Catalyzed by MoO₂X₂L Complexes: A DFT Mechanistic Study. *Dalton Trans.* **2006**, *11*, 1383–1389. [[CrossRef](#)] [[PubMed](#)]

48. Herbert, M.; Montilla, F.; Álvarez, E.; Galindo, A. New Insights into the Mechanism of Oxodiperoxomolybdenum Catalysed Olefin Epoxidation and the Crystal Structures of Several Oxo-Peroxo Molybdenum Complexes. *Dalton Trans.* **2012**, *41*, 6942. [[CrossRef](#)] [[PubMed](#)]
49. Morlot, J.; Uyttebroeck, N.; Agustin, D.; Poli, R. Solvent-Free Epoxidation of Olefins Catalyzed by “[MoO₂(SAP)]”: A New Mode of tert-Butyl hydroperoxide Activation. *ChemCatChem* **2013**, *5*, 601–611. [[CrossRef](#)]
50. Calhorda, M.J.; Costa, P.J. Unveiling the Mechanisms of Catalytic Oxidation Reactions Mediated by Oxo-Molybdenum Complexes: A Computational Overview. *Curr. Org. Chem.* **2012**, *16*, 65–72. [[CrossRef](#)]
51. Lempers HE, B.; Van Crey, M.J.; Sheldon, R.A. Molybdenum-Catalyzed Epoxidations of Oct-1-ene and Cyclohexene with Organic Hydroperoxides: Steric Effects of the Alkyl Substituents of the Hydroperoxide on the Reaction Rate. *Recl. Trav. Chim. Pays-Bas* **1996**, *115*, 542–546. [[CrossRef](#)]
52. Sharbatdaran, M.; Farzaneh, F.; Larijani, M.M. Epoxidation of Alkenes Using Inorganic Polymer of Silica Zirconia Molybdate as Catalyst. *J. Mol. Catal. A Chem.* **2014**, *382*, 79–85. [[CrossRef](#)]
53. Shen, Y.; Jiang, P.; Zhang, J.; Bian, G.; Zhang, P.; Dong, Y. Highly Dispersed Molybdenum Incorporated Hollow Mesoporous Silica Spheres as an Efficient Catalyst on Epoxidation of Olefins. *Mol. Catal.* **2017**, *433*, 212–223. [[CrossRef](#)]
54. Zhang, J.; Zhang, H.; Liu, L.; Chen, Z. The Interaction of Molybdenum and Titanium in Mesoporous Materials for Olefin Epoxidation. *React. Kinet. Mech. Catal.* **2022**, *135*, 317–331. [[CrossRef](#)]
55. Wang, P.; Zhao, J.; Li, X.; Yang, Y.; Yang, Q.; Li, C. Assembly of ZIF Nanostructures around Free Pt Nanoparticles: Efficient Size-Selective Catalysts for Hydrogenation of Alkenes under Mild Conditions. *Chem Comm.* **2013**, *49*, 3330–3332. [[CrossRef](#)]
56. Lin, L.; Zhang, T.; Zhang, X.; Liu, H.; Yeung, K.L.; Qiu, J. New Pd/SiO₂@ZIF-8 Core-Shell Catalyst with Selective, Antipoisoning, and Antileaching Properties for the Hydrogenation of Alkenes. *Ind. Eng. Chem. Res.* **2014**, *53*, 10906–10913. [[CrossRef](#)]
57. Zhang, J.; Zhao, Y.; Li, A.; Ye, H.; Shang, Q.; Shi, X.; Shen, Y. Enhanced Catalytic Activity over Mo-Containing Hierarchical Macro-Mesoporous SBA-15 Catalysts for Epoxidation of Olefins. *J. Porous Mater.* **2019**, *26*, 869–880. [[CrossRef](#)]
58. Lima, S.; Antunes, M.M.; Fernandes, A.; Pillinger, M.; Ribeiro, M.F.; Valente, A.A. Catalytic Cyclodehydration of Xylose to Furfural in the Presence of Zeolite H-Beta and a Micro/Mesoporous Beta/TUD-1 Composite Material. *Appl. Catal. A Gen.* **2010**, *388*, 141–148. [[CrossRef](#)]
59. Mahtabani, A.; La Zara, D.; Anyszka, R.; He, X.; Paajanen, M.; van Ommen, J.R.; Dierkes, W.; Blume, A. Gas Phase Modification of Silica Nanoparticles in a Fluidized Bed: Tailored Deposition of Aminopropylsiloxane. *Langmuir* **2021**, *37*, 4481–4492. [[CrossRef](#)] [[PubMed](#)]